AGU PUBLICATIONS

JGR

Journal of Geophysical Research: Atmospheres

RESEARCH ARTICLE
10.1002/2016JD025623

Key Points:
- Two decades will be needed for $PM_{2.5}$ in key polluted regions to drop below 35 $\mu g\,m^{-3}$ under all RCPs
- Concentrations of $PM_{2.5}$ fall by 38-58% in 2050 relative 2000 over the four polluted areas under RCP2.6 and RCP4.5
- Averaged over east China, changes in aerosols lead to positive DRF of 1.22 (1.88) W m^{-2} in 2050 relative 2000 under RCP2.6 (RCP4.5)

Supporting Information:
- Supporting Information S1

Correspondence to:
H. Liao,
hongliao@nuist.edu.cn

Citation:
Li, K., H. Liao, J. Zhu, and J. M. Moch (2016), Implications of RCP emissions on future $PM_{2.5}$ air quality and direct radiative forcing over China, *J. Geophys. Res. Atmos.*, *121*, 12,985–13,008, doi:10.1002/2016JD025623.

Received 7 JUL 2016
Accepted 8 SEP 2016
Accepted article online 11 SEP 2016
Published online 8 NOV 2016

Implications of RCP emissions on future $PM_{2.5}$ air quality and direct radiative forcing over China

Ke Li[1,2], Hong Liao[3,4], Jia Zhu[1,2], and Jonathan M. Moch[5]

[1]State Key Laboratory of Atmospheric Boundary Layer Physics and Atmospheric Chemistry, Institute of Atmospheric Physics, Chinese Academy of Sciences, Beijing, China, [2]University of Chinese Academy of Sciences, Beijing, China, [3]School of Environmental Science and Engineering, Nanjing University of Information Science and Technology, Nanjing, China, [4]Joint International Research Laboratory of Climate and Environment Change, Nanjing University of Information Science and Technology, Nanjing, China, [5]Department of Earth and Planetary Sciences, Harvard University, Cambridge, Massachusetts, USA

Abstract Severe $PM_{2.5}$ air pollution in China and the First Grand National Standard (FGNS), implemented in 2016 (annual $PM_{2.5}$ concentration target of less than 35 $\mu g\,m^{-3}$), necessitate urgent reduction strategies. This study applied the nested-grid version of the Goddard Earth Observing System (GEOS) chemical transport model (GEOS-Chem) to quantify 2000–2050 changes in $PM_{2.5}$ air quality and related direct radiative forcing (DRF) in China, based on future emission changes under the representative concentration pathway (RCP) scenarios of RCP2.6, RCP4.5, RCP6.0, and RCP8.5. In the near term (2000–2030), a projected maximum increase in $PM_{2.5}$ concentrations of 10–15 $\mu g\,m^{-3}$ is found over east China under RCP6.0 and RCP8.5 and less than 5 $\mu g\,m^{-3}$ under RCP2.6 and RCP4.5. In the long term (2000–2050), $PM_{2.5}$ pollution clearly improves, and the largest decrease in $PM_{2.5}$ concentrations of 15–30 $\mu g\,m^{-3}$ is over east China under all RCPs except RCP6.0. Focusing particularly on highly polluted regions, we find that Beijing-Tianjin-Hebei (BTH) wintertime $PM_{2.5}$ concentrations meeting the FGNS occur after 2040 under RCP2.6, RCP4.5, and RCP8.5, and summertime $PM_{2.5}$ concentrations reach this goal by 2030 under RCP2.6 and RCP4.5. In Sichuan Basin (SCB), wintertime $PM_{2.5}$ concentrations below the FGNS occur only in 2050 under RCP2.6 and RCP4.5, although future summertime $PM_{2.5}$ will be well controlled. The difficulty in controlling future $PM_{2.5}$ concentrations relates to unmitigated high levels of nitrate, although NO_x and SO_2 emissions show substantial reductions during 2020–2040. The changes in aerosol concentrations lead to positive aerosol DRF over east China (20°–45°N, 100°–125°E) by 1.22, 1.88, and 0.66 W m^{-2} in 2050 relative to 2000 under RCP2.6, RCP4.5, and RCP8.5, respectively. When considering both health and climate effects of $PM_{2.5}$ over China, for example, $PM_{2.5}$ concentrations averaged over east China under RCP4.5 (RCP2.6) decrease by 54% (43%) in 2050 relative to 2000, but at the cost of warming with DRF of 1.88 (1.22) W m^{-2}. Our results indicate that it will be possible to mitigate future $PM_{2.5}$ pollution in China, but it will likely take two decades for polluted regions such as BTH and SCB to meet the FGNS, based on all RCP scenarios. At the same time, the consequent warming effects from reduced aerosols are also significant and inevitable.

1. Introduction

Fine particulate matter with a diameter of 2.5 μm or less ($PM_{2.5}$) is a major air pollutant that affects human health [*Lelieveld et al.*, 2015] and atmospheric visibility [*Wang et al.*, 2009], as well as regional and global climate change [Intergovernmental Panel on Climate Change (*IPCC*), 2013]. In China, with rapid industrialization and urbanization over the past several decades, concentrations of major $PM_{2.5}$ components (sulfate, nitrate, ammonium, black carbon (BC), organic carbon (OC), and mineral dust) are at considerably high levels [*Qu et al.*, 2010; *Cao et al.*, 2012; *Zhang et al.*, 2012; *Jiang et al.*, 2015; *Wang et al.*, 2015]. For example, in January 2013, over the Beijing-Tianjin-Hebei (BTH) region, monthly mean and daily maximum $PM_{2.5}$ concentrations reached ~200 $\mu g\,m^{-3}$ and 700 $\mu g\,m^{-3}$, respectively [*Jiang et al.*, 2015]. Thus, the focus of attention on air pollution induced by high $PM_{2.5}$ concentrations is rising in China, with both the general public and the scientific community, where the need to reduce emissions of primary air pollutants and precursors is a recognized concern [*Wang and Hao*, 2012; *Guo et al.*, 2014; *He et al.*, 2014; *R.-J. Huang et al.*, 2014; *Zhuang et al.*, 2014; *Gao et al.*, 2015; *Kelly and Zhu*, 2016].

The representative concentration pathways (RCPs) [*van Vuuren et al.*, 2011], in support of the Fifth Assessment Report of the Intergovernmental Panel on Climate Change (IPCC), include estimates of air

pollutants and precursors spanning from 2000 to 2100 under a range of warming scenarios. These future scenarios, denoted as RCP2.6, RCP4.5, RCP6.0, and RCP8.5, represent global radiative forcings of 2.6, 4.5, 6.0, and 8.5 W m^{-2} in 2100 relative to preindustrial times, respectively. The projected air quality based on future emission scenarios in the next several decades has emerged as an important topic of interest for the scientific community [e.g., *Carmichael et al.*, 2009; *Butler et al.*, 2012; *Kelly et al.*, 2012; *Colette et al.*, 2013; *Trail et al.*, 2014; *Lapina et al.*, 2015; *Val Martin et al.*, 2015]. Using Canadian climate models and a regional air-quality modeling system (A Unified Regional Air-quality Modeling System), *Kelly et al.* [2012] reported a large midcentury decrease (up to 3–10 μg m^{-3}) in summer $PM_{2.5}$ relative to the present day over the eastern United States (U.S.) under the RCP6.0 and SRES (Special Report on Emissions Scenarios) A2 climate. *Colette et al.* [2013] predicted that decrease in $PM_{2.5}$ concentrations by 2050 in western Europe attributed to air pollutant emissions could reach up to 60% under a reference scenario (resembling RCP8.5) and 75% under a mitigation scenario (resembling RCP2.6). Most recently, *Val Martin et al.* [2015], using the Community Earth System Model, also projected $PM_{2.5}$ concentrations to show a future decrease (4 μg m^{-3} and 2 μg m^{-3}, by 2050, over the eastern and western U.S., respectively), under both RCP4.5 and RCP8.5. Such findings assist policymakers in identifying mitigation targets for the improvement of future regional air quality.

Several studies have differentiated the relative importance between climate change and emission changes when assessing future changes in $PM_{2.5}$ air quality [e.g., *Tagaris et al.*, 2007; *Lam et al.*, 2011; *Kelly et al.*, 2012; *Colette et al.*, 2013; *Jiang et al.*, 2013; *Val Martin et al.*, 2015]. Specifically, they confirm a primary role played by emission changes, although climate change has the potential to abate $PM_{2.5}$ pollution or counteract reduction efforts by altering meteorological variables (e.g., precipitation, temperature, wind, relative humidity, and boundary layer height), as well as the occurrence of stagnation episodes, to influence the emission, formation, transport, and removal of aerosols [*Liao et al.*, 2006; *Jacob and Winner*, 2009; *Fiore et al.*, 2012; *West et al.*, 2013; *Horton et al.*, 2014]. For example, *Lam et al.* [2011] pointed out that 90% of the predicted future decline (by 2050) in $PM_{2.5}$ concentrations over the U.S. will be contributed by emission reductions, with climate change only expected to account for around 10%. *Colette et al.* [2013] concluded that the main factor affecting future $PM_{2.5}$ air quality in Europe is air pollutant emissions, rather than climate change or intercontinental transport. Similarly, *Val Martin et al.* [2015] also reported that changes in anthropogenic emissions could account for more than 95% of projected decreases in $PM_{2.5}$ concentrations by 2050 all the entire U.S., while climate change may slightly offset the benefits of emission reductions. Moreover, *Fiore et al.* [2012] reviewed studies on the interaction between global climate and air quality and indicated that the ranges in projections of air quality throughout the 21st century are mainly driven by emission changes rather than by climate change—a notion also adopted in the 2013 IPCC report [*Kirtman et al.*, 2013].

Only a few studies have investigated the impacts of future emission changes on projected $PM_{2.5}$ air quality over China. *Carmichael et al.* [2009] estimated how $PM_{2.5}$ (including carbonaceous aerosols and sulfate only) over Asia may change by 2030, based on a regional chemical transport model (Sulfur Transport and Deposition Model), with future emission scenarios and fixed present-day meteorology. They predicted that annual mean $PM_{2.5}$ concentrations could increase by more than 15 μg m^{-3} over populated eastern China under the SRES A1B scenario, while the SRES B1 scenario only showed a slight increase (0.5–2 μg m^{-3}) over China. Using the Community Multi-scale Air Quality Model, *Xing et al.* [2011] reported that $PM_{2.5}$ concentrations by 2020 will decrease by 16% relative to 2005 over China under a scenario of improved energy efficiencies and strict legislation but will increase by 8% under a scenario of current control legislation and implementation status. Using the global chemical transport model (GEOS-Chem) driven by the version 3 of the Goddard Institute for Space Studies General Circulation Model (GCM) at a resolution of 4° × 5°, *Jiang et al.* [2013] predicted that $PM_{2.5}$ concentrations in eastern China would reduce by 1–8 μg m^{-3} over 2000–2050, under the SRES A1B scenario, due to changes in emissions. However, these studies failed to provide much information on either future regional and local $PM_{2.5}$ air quality or related evolution trends over China, partly due to limited model resolution or an incomplete chemical mechanism for the formation of aerosols (e.g., nitrate).

Climatic effects of air pollutants should be considered simultaneously when developing emission reduction policies to improve air quality [*Leibensperger et al.*, 2012; *Liao et al.*, 2015; *Turnock et al.*, 2016]. Using a regional climate model with off-line aerosols (sulfate, OC, BC, mineral dust, and sea salt), *Qian et al.* [2003] quantified annual mean direct radiative forcing (DRF) at the top of the atmosphere (TOA) of total aerosols to be

$-5.11\,W\,m^{-2}$ in eastern China (21°–37°N, 110°–120°E) and $-6.77\,W\,m^{-2}$ in the Sichuan Basin (SCB). *Chang and Liao* [2009] estimated the annual mean DRF of anthropogenic sulfate, nitrate, BC, and OC at the TOA to be −2.50, −0.75, +0.58, and $-0.13\,W\,m^{-2}$, respectively, averaged over eastern China (18°–45°N, 95°–125°E), based on a GCM with online simulations of gas-phase chemistry and aerosols. These DRF estimates are vastly different, resulting from emissions and chemistry scheme in the models as well as the treatments of aerosol optical properties (e.g., mixing state and aging process). The evolution of future aerosol DRF in China could be pronounced under conditions of improved air quality. *Li et al.* [2014] studied the decadal variations of radiative forcing of anthropogenic aerosols for the period of 1850–2100 and showed that TOA aerosol DRF in East Asia (20°–45°N, 100°–145°E) will reach a maximum of $-1.21\,W\,m^{-2}$ by the 2020s, before decreasing to only $-0.2\,W\,m^{-2}$ by the end of this century under RCP8.5. *Westervelt et al.* [2015] concluded that 30–40% of total climate warming in East Asia by 2100 under RCP8.5 will result from reduced aerosol. Furthermore, to our knowledge, few studies have quantified the changes in aerosol radiative forcing when emission reduction measures are taken.

Building upon our related work in which we focused on future ozone (O_3) air quality over China [*Zhu and Liao*, 2016], here we examine future (2000–2050) $PM_{2.5}$ concentrations and associated DRF in China driven by different RCP emission scenarios with fixed meteorology for the year 2010, using the nested-grid version of GEOS-Chem model with a high resolution of $0.5° \times 0.667°$. We aim to quantify (1) the possible ranges of $PM_{2.5}$ concentrations over the period of 2000–2050 under the various RCPs, (2) how $PM_{2.5}$ components vary in cases of changed emissions, and (3) the corresponding evolution of future aerosol DRF. We do not include any changes in climate that would also affect future $PM_{2.5}$ concentrations; instead, we focus on the impacts of anthropogenic emission changes alone, which is the primary target for improving $PM_{2.5}$ air quality in China. A description of GEOS-Chem model, the RCP emission scenarios, and the numerical simulations is provided in section 2. In section 3, simulated present-day $PM_{2.5}$ levels are compared with measurements. Section 4 describes the projected changes in $PM_{2.5}$ air quality under the RCP scenarios, especially over polluted regions. Section 5 presents the projected evolution of aerosol DRF. Section 6 discusses some implications that may be useful for policymakers. Conclusions are given in section 7.

2. Model Description, Emissions, and Numerical Experiments

2.1. GEOS-Chem Model

We simulated $PM_{2.5}$ components in China by using the nested-grid capability of GEOS-Chem model (version 9-01-03; http://acmg.seas.harvard.edu/geos/) driven by assimilated meteorological data from the Goddard Earth Observing System (GEOS) of NASA's Global Modeling and Assimilation Office [*Chen et al.*, 2009]. The simulation domain was nested over Asia (11°S–55°N, 70°–150°E), with a horizontal resolution of $0.5° \times 0.667°$ and 47 vertical layers up to 0.01 hPa. Tracer concentrations at the lateral boundaries were provided by global GEOS-Chem simulations at a horizontal resolution of $4° \times 5°$ and updated every 3 h.

GEOS-Chem model includes fully coupled O_3-NO_x-hydrocarbon chemistry and aerosols, including sulfate [*Park et al.*, 2004], nitrate [*Pye et al.*, 2009], ammonium, OC and BC [*Park et al.*, 2003], mineral dust [*Fairlie et al.*, 2007], and sea salt [*Alexander et al.*, 2005]. Wet deposition of soluble aerosols and gases follows the scheme of *Liu et al.* [2001], and dry deposition follows the standard resistance-in-series model of *Wesely* [1989]. In this study, we focus on changes of future anthropogenic $PM_{2.5}$ levels; thus, mineral dust and sea-salt aerosols are not included in the total $PM_{2.5}$ concentrations. Secondary organic aerosol (SOA) is also excluded, because a large fraction (~70%) of SOA formation in China happens through oxidizing biogenic volatile organic compounds (BVOCs) [*Fu et al.*, 2012; *Fu and Liao*, 2012]. BVOC emissions were kept constant because we fixed meteorological fields at year 2010 in simulations, but anthropogenic changes in oxidants might influence SOA formation [*Shilling et al.*, 2013; *Xu et al.*, 2015; *Rattanavaraha et al.*, 2016].

The all-sky aerosol DRF at the TOA was calculated via the Rapid Radiative Transfer Model for GCMs (RRTMG), which has been coupled online with GEOS-Chem model [*Heald et al.*, 2014]. The RRTMG solves the radiative transfer equation in 14 shortwave bands and 16 longwave bands, covering 230 nm through 56 μm. We calculated instantaneous shortwave and longwave radiative fluxes every 3 h. The sizes and optical properties of aerosol species followed the methods of *Heald et al.* [2014]. The differences in radiative flux with and

without aerosols are often referred to as the aerosol direct radiative effect (DRE). The DRF of aerosols can be estimated by differentiating the DRE simulated with and without the presence of anthropogenic aerosols.

2.2. Emissions

Global anthropogenic emissions of air pollutants (NO_x, carbon monoxide, nonmethane VOCs, sulfur dioxide (SO_2), ammonia (NH_3), BC, and OC) for each decadal time slice over the period of 2000–2050 under the RCP scenarios were obtained from http://www.iiasa.ac.at/web-apps/tnt/RcpDb and then implemented into GEOS-Chem model. The native RCP emissions, with a gridded $0.5° \times 0.5°$ resolution, included 10 anthropogenic emission activities (surface transport, shipping, aviation, energy production and distribution, industrial combustion, residential and commercial fuel use, solvent use, waste management and disposal, agriculture, and agricultural waste burning), and two biomass burning types (grass fires and forest fires).

RCP emissions are generally annual mean values, except for biomass burning, shipping, and aircraft emissions, which have monthly variations. To better simulate aerosols over China, we obtained monthly scaling factors for O_3 precursors, aerosol precursors, and aerosols, from version 2 of the EDGAR (Emission Database for Global Atmospheric Research) Hemispheric Transport of Air Pollution (HTAP) data set for the year 2010 [*Janssens-Maenhout et al.*, 2015], and applied these gridded monthly scaling factors to the RCP anthropogenic emissions for all years and RCP scenarios. Anthropogenic emissions over China from HTAP are mainly based on the most recent inventory (the Multi-resolution Emission Inventory for China: http://www.meicmodel.org), which has been widely used in modeling aerosols over China [e.g., *X. Huang et al.*, 2014; *L. T. Wang et al.*, 2014; *Huang et al.*, 2015; *Zhang et al.*, 2015a, 2015b; *Wang et al.*, 2016]. The ratios between maximum and minimum monthly emissions of SO_2, NO_x, BC, and OC in China from HTAP are 1.39, 1.31, 2.11, and 2.84, respectively, which are very close to the values of 1.36, 1.27, 2.11, and 2.81 from the Intercontinental Chemical Transport Experiment Phase B inventory [*Zhang et al.*, 2009]. Monthly variations of NH_3 emissions in China from HTAP are also in good agreement with those compiled by the study of *Paulot et al.* [2014].

The evolutions of anthropogenic emissions for SO_2, NO_x, NH_3, BC, and OC over 2000–2050 in China under the RCP scenarios are shown in Figure 1. Total anthropogenic emissions of SO_2, NO_x, NH_3, BC, and OC over China in 2000 are 18.1, 11.6, 6.4, 1.3, and 2.9 Tg species yr^{-1}, respectively. Over 2000–2050, the evolutions of all species except NH_3 experience a similar pattern of peak emissions occurring in 2010 or 2020, and a large reduction in emissions appearing during 2030–2050, under RCP2.6, RCP4.5, and RCP8.5. SO_2 emissions are lowered by 86%, 80%, and 69% in 2050 relative to 2000, respectively, under RCP2.6, RCP4.5, and RCP8.5. Relative to 2000, NO_x emissions in 2020 (2050) increase (decrease) by 55% (36%), 54% (50%), and 132% (1%), respectively, under RCP2.6, RCP4.5, and RCP8.5. BC (OC) emissions in 2050 decrease by 60–96% (60–80%), compared with those in 2000, under these three RCPs. Interestingly, under RCP6.0, all of the emissions hold an increasing trend. By 2050, emissions of SO_2, NO_x, BC, and OC have increased by 38%, 113%, 43%, and 41%, respectively. It should be noted that although the RCP6.0 scenario in China seems to be unmitigated over 2000–2050, its emissions drop sharply after 2050, as one would expect (supporting information of *IPCC* [2013]). NH_3 emissions increase steadily from 2000 to 2050 (by 35–81%) under all the RCP scenarios, which will mainly be due to the increased population and food demand [*van Vuuren et al.*, 2011].

Natural emissions follow the configurations in the standard GEOS-Chem simulation and are all fixed at the year 2010. Lightning NO_x emissions were described by *Sauvage et al.* [2007] and *Murray et al.* [2012], and soil NO_x by *Yienger and Levy* [1995]. NH_3 emissions from soil, vegetation, and the oceans were from the Global Emissions Inventory Activity inventory [*Bouwman et al.*, 1997]. BVOC emissions were calculated from the Model of Emissions of Gases and Aerosols from Nature [*Guenther et al.*, 2006]. Natural emissions of BVOCs, lightning NO_x, and soil NO_x emissions over China were dependent on year 2010 meteorology, which are 18.07 Tg C yr^{-1}, 0.30 Tg N yr^{-1}, and 0.26 Tg N yr^{-1}, respectively.

2.3. Numerical Simulations

An overview of the numerical experiments is already provided in *Zhu and Liao* [2016]; thus, only a brief description is provided here. Simulations were performed with present-day emissions (year 2000) and future emissions (years 2010, 2020, 2030, 2040, and 2050) for each of the four RCP scenarios. All of the simulations were driven by the assimilated GEOS-5 meteorology of the year 2010. Since we aim to simulate future $PM_{2.5}$ air quality with 2010, 2020, 2030, 2040, and 2050 emissions, year 2010 is selected considering that 2010 has

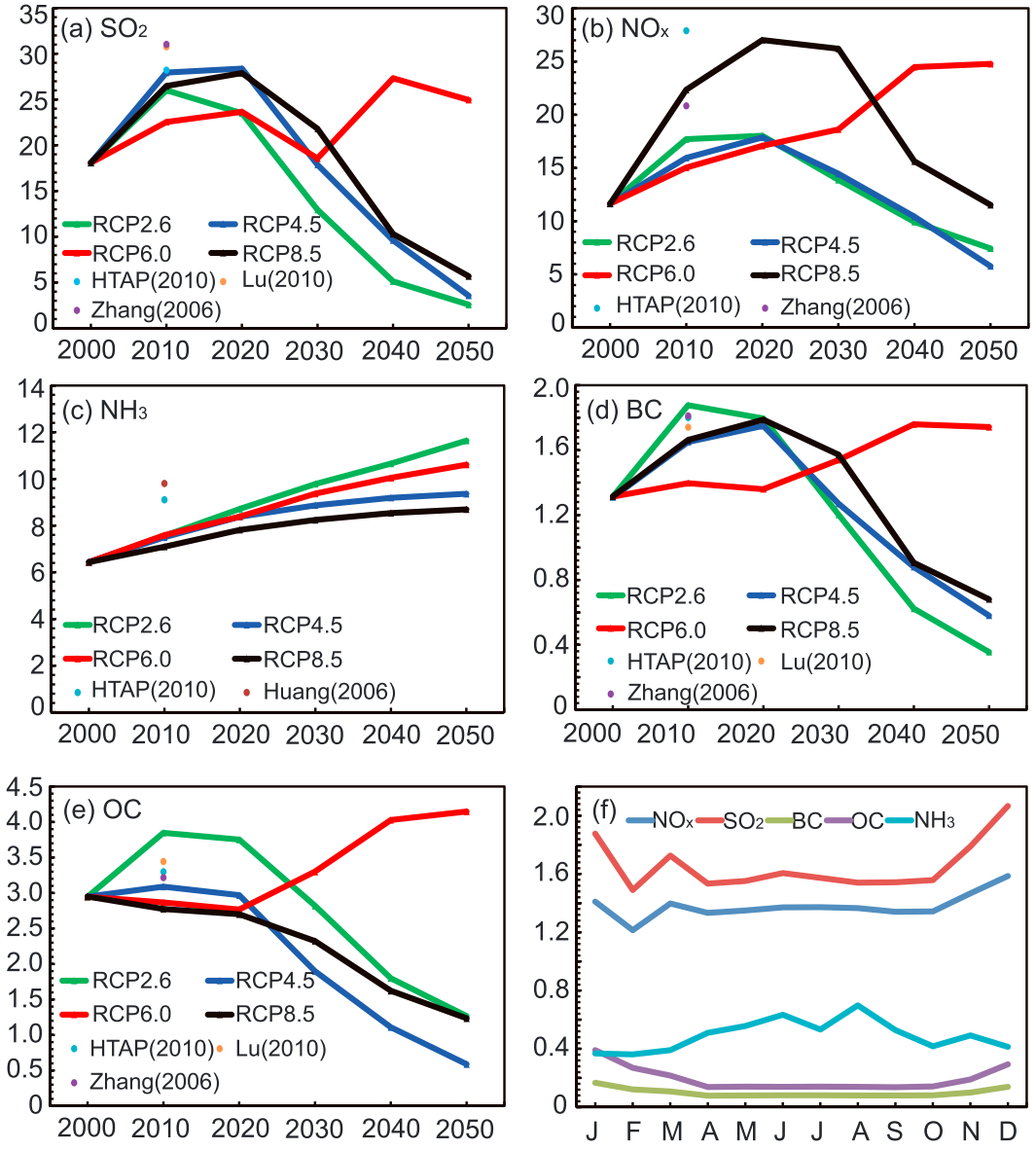

Figure 1. Anthropogenic emissions (units: Tg species yr^{-1}) of (a) SO_2, (b) NO_x, (c) NH_3, (d) BC, and (e) OC in China for the period of 2000–2050 under the four RCP scenarios (different colored lines). Recent emission inventories of aerosols and aerosol precursors (different colored dots) for the years 2010 or 2006 are also shown in Figures 1a–1e (HTAP [*Zhang et al.*, 2009; *Lu et al.*, 2011; *Huang et al.*, 2012]), and all of these emissions are listed at year 2010 in comparison of those under RCP scenarios. (f) Monthly variations of anthropogenic emissions for aerosols and aerosol precursors (units: Tg species $month^{-1}$) in China for the year 2010 from the HTAP inventory.

the most realist present-day meteorology among these years. Simulated concentrations of $PM_{2.5}$ and its components with meteorology of 2010 compare very well with those simulated with consecutive 5 year (2008–2012) meteorology (see Figure S1 in the supporting information). Each of the simulations was integrated for 18 months, and the first 6 months were treated as model initialization for both the nested high-resolution (0.5° × 0.667°) and global (4° × 5°) simulations that provided the boundary conditions.

3. Simulated Current $PM_{2.5}$ Levels Over China and Model Evaluation

GEOS-Chem model has been extensively applied to reproduce observed $PM_{2.5}$ concentrations and their components (including sulfate, nitrate, ammonium, BC, and OC) over China [e.g., *Zhang et al.*, 2010; *Fu et al.*, 2012;

Jiang et al., 2013; *Lou et al.*, 2014; *Mu and Liao*, 2014; *Yang et al.*, 2015; *Li et al.*, 2016; *Mao et al.*, 2016]. In this section, we evaluate the ability of GEOS-Chem simulations driven by current (year 2010) RCP emissions to reproduce the spatial distributions and seasonal variations of observed current surface-layer $PM_{2.5}$ concentrations. Figure 1 presents the current emissions of SO_2, NO_x, NH_3, BC, and OC in China from several of the latest inventories [*Zhang et al.*, 2009; *Lu et al.*, 2011; *Huang et al.*, 2012; *Janssens-Maenhout et al.*, 2015]. These aforementioned emission inventories are widely adopted in modeling aerosols over China. Compared with these inventories, current NO_x emissions in China are underestimated by all the RCPs in 2010. Current emissions of SO_2 and BC are in good agreement with those from the 2010 emissions of RCPs, except RCP6.0. All the RCPs in 2010 except RCP2.6 underestimate current OC emissions in China, while OC emissions are highly overestimated under RCP2.6. Current NH_3 emissions are underestimated by all the RCPs. Here we mainly show the simulated surface-layer $PM_{2.5}$ concentrations driven by 2010 emissions under RCP4.5, which is seemingly the closest scenario to current emission inventories.

3.1. Simulated Surface-Layer $PM_{2.5}$ Concentrations

Figure 2 shows the simulated seasonal mean concentrations of sulfate, nitrate, ammonium, BC, OC, and $PM_{2.5}$ (sum of sulfate, nitrate, ammonium, BC, and OC) over China from the simulation driven by 2010 emissions of RCP4.5. The highest seasonal mean concentrations of $PM_{2.5}$ over the North China Plain (NCP) are 70–80 $\mu g\ m^{-3}$ in DJF (December-January-February), followed by 50–60 $\mu g\ m^{-3}$ in SON (September-October-November), 40–50 $\mu g\ m^{-3}$ in JJA (June-July-August), and 30–40 $\mu g\ m^{-3}$ in MAM (March-April-May), respectively. Over the SCB, the highest $PM_{2.5}$ concentrations are more than 80 $\mu g\ m^{-3}$ in DJF, but decrease to only 30–50 $\mu g\ m^{-3}$ for the other three seasons. The simulated regions with high $PM_{2.5}$ concentrations in China are consistent with where haze pollution episodes have frequently happened during recent years [*Zhang et al.*, 2012; *Wang et al.*, 2015]. The seasonal variations of $PM_{2.5}$ concentrations also agree well with previous model results [e.g., *Fu et al.*, 2012; *Wang et al.*, 2013; *Lou et al.*, 2014; *Mu and Liao*, 2014].

The simulated sulfate concentrations over the NCP are 15–20 $\mu g\ m^{-3}$ in JJA, due to strong photochemistry during this season, while sulfate over south China demonstrates low concentrations of 4–8 $\mu g\ m^{-3}$ in JJA as a result of enhanced wet removal associated with Asian summer monsoon precipitation [*Zhang et al.*, 2010]. In DJF, high concentrations of sulfate (20–25 $\mu g\ m^{-3}$) are found over the SCB, owing to large SO_2 emissions from the residential sector for winter heating. High nitrate concentrations are simulated over the NCP, with 15–20 $\mu g\ m^{-3}$ in DJF and SON, and 8–15 $\mu g\ m^{-3}$ in JJA and MAM. This seasonal variation could be explained by the low temperatures in DJF and SON favoring nitrate ammonium formation, and its formation in JJA is enhanced by high emissions of NH_3 [*Huang et al.*, 2012]. Simulated ammonium concentrations are 6–10 $\mu g\ m^{-3}$ over the NCP throughout the year and show high values of 10–15 $\mu g\ m^{-3}$ over the SCB in DJF. The maximum concentrations of BC and OC reach 10 and 20–25 $\mu g\ m^{-3}$, respectively, over both the NCP and SCB in DJF. Meanwhile, their low values are both found in JJA, due to decreased emissions and enhanced wet scavenging by monsoon precipitation [*Zhang et al.*, 2010; *Fu et al.*, 2012].

3.2. Comparison of Simulated Concentrations With Measurements

Figure 3 shows the simulated spatial distribution of annual mean surface-layer $PM_{2.5}$ concentrations under the 2010 emissions of RCP4.5. Also shown are observations from an aerosol measurement network (China Atmosphere Watch Network (CAWNET)) that produced monthly measurements of surface mass concentrations of PM_{10} components at 14 sites for the period 2006–2007 [*Zhang et al.*, 2012]. This set of measurements has been widely applied to evaluate modeled aerosol concentrations in China [e.g., *Fu et al.*, 2012; *Jiang et al.*, 2013; *Lou et al.*, 2014; *Wang et al.*, 2013; *Gao et al.*, 2014; *Huang et al.*, 2015; *Zhang et al.*, 2015a; *Li et al.*, 2016]. For comparison purposes, we converted the observed PM_{10} to $PM_{2.5}$ by multiplying by 0.6, based on the suggestion in *Zhang et al.* [2002]. It can be seen that observed high values of $PM_{2.5}$ over the NCP and SCB, though underestimated, are generally reflected in the GEOS-Chem simulations.

Figure 4 compares simulated monthly mean $PM_{2.5}$ concentrations for the year 2010 under RCP scenarios with observed values at five sites (Gucheng, Zhengzhou, Linan, Panyu, and Chengdu) from CAWNET, which are all located in polluted regions (defined in section 4.2). At Gucheng, observed seasonal variations of $PM_{2.5}$ concentrations are generally captured, except for low biases from October to February. The observed magnitude and seasonal variations of $PM_{2.5}$ concentrations at Zhengzhou are better reproduced than those at Gucheng. Simulated $PM_{2.5}$ concentrations at Linan and Panyu are in very good agreement with those from

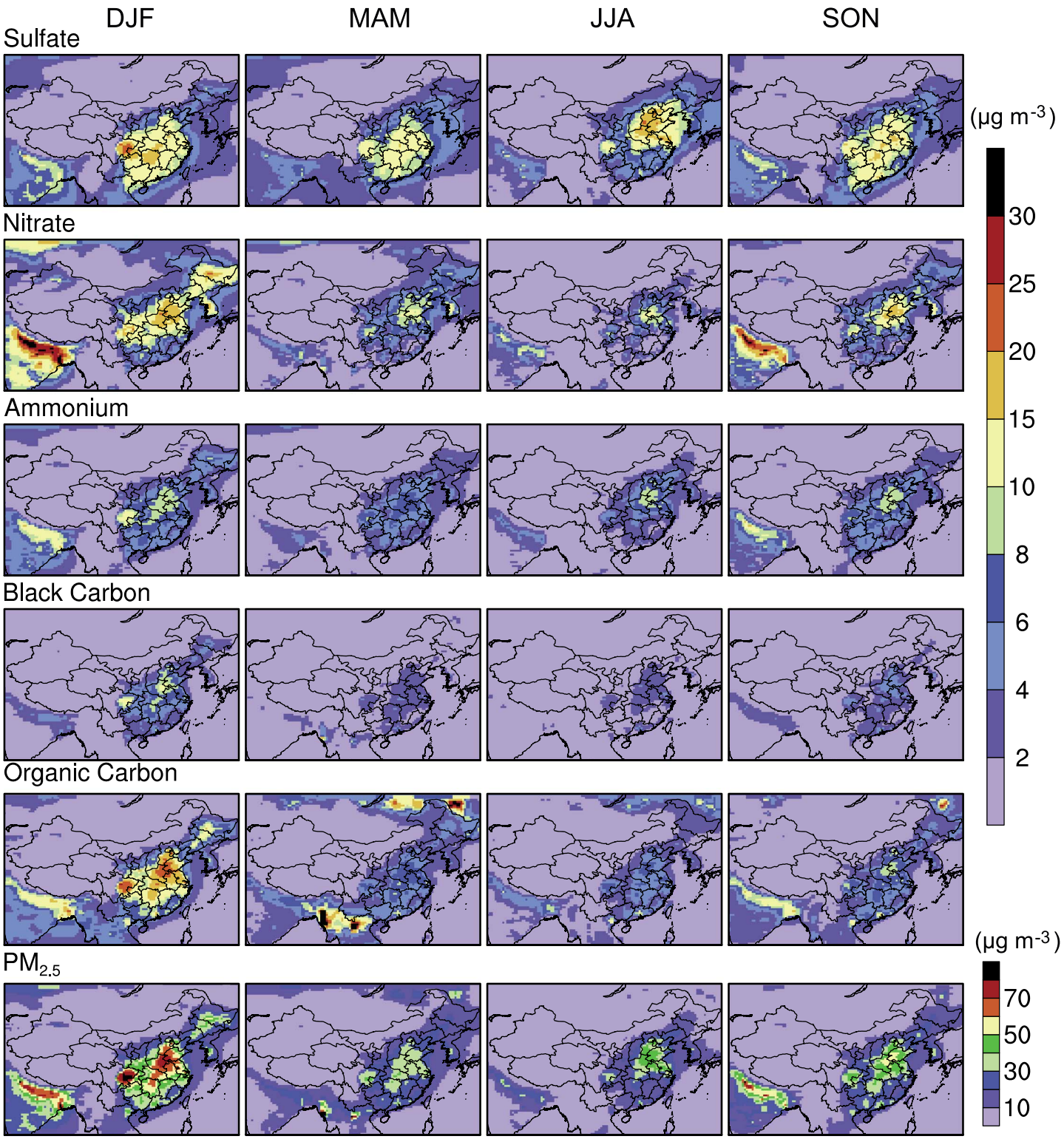

Figure 2. Simulated seasonal mean surface-layer concentrations (units: $\mu g\,m^{-3}$) of sulfate, nitrate, ammonium, BC, OC, and $PM_{2.5}$ (sum of sulfate, nitrate, ammonium, BC, and OC) for year 2010 under RCP4.5 emissions.

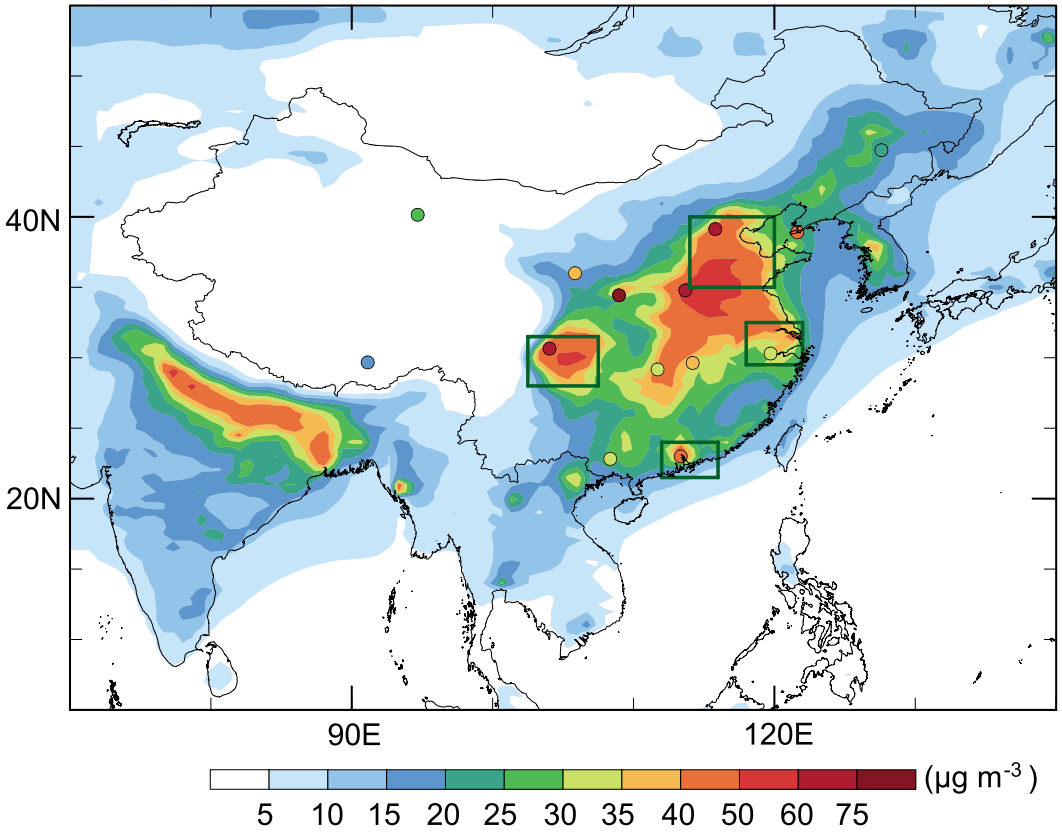

Figure 3. Simulated annual mean $PM_{2.5}$ concentrations (units: $\mu g\,m^{-3}$) for the year 2010 under RCP4.5 emissions. The colored circles denote the annual mean $PM_{2.5}$ concentrations measured at 14 sites of the China Atmosphere Watch Network (CAWNET) [*Zhang et al.*, 2012] during 2006–2007. Four polluted regions are highlighted by green rectangles: Beijing-Tianjin-Hebei (BTH, 35°–40°N, 114°–120°E), Yangtze River Delta (YRD, 29.5°–32.5°N, 118°–122°E), Pearl River Delta (PRD, 21°–23.5°N, 112°–116°E), and Sichuan Basin (SCB, 28°–31.5°N, 102.5°–107.5°E).

observations. At Chengdu, the model can successfully capture the observed $PM_{2.5}$ concentrations in winter, and low biases are found in the simulation during the other seasons. This underestimation can be partly explained by the observed high ratios of secondary OC in total OC [*Zhang et al.*, 2012] and the omission of SOA in the simulations. It is also noted that simulated $PM_{2.5}$ concentrations at these five sites are highly consistent with each other under different RCP scenarios.

A comparison of seasonal mean concentrations of $PM_{2.5}$ and their components between the simulations and observations at 14 CAWNET is given in Figure 5. Scatterplots of simulated versus observed $PM_{2.5}$ components exhibit high correlation coefficients for sulfate ($r = 0.69$), nitrate ($r = 0.68$), ammonium ($r = 0.73$), and BC ($r = 0.53$), but a relatively low value ($r = 0.29$) for OC. Table S1 in the supporting information shows correlation coefficient and normalized mean biases (NMBs) for observed and simulated seasonal mean $PM_{2.5}$ and its components. For $PM_{2.5}$, the lowest (highest) bias of −31% (−44%) is found in DJF (JJA), while the highest r of 0.7 occurs in SON. As for sulfate-nitrate-ammonium (SNA) aerosol, simulated sulfate (nitrate) exhibits highest NMB of −47% (−39%) in DJF (JJA). Model performance is better in simulating BC than OC. Overall, total $PM_{2.5}$ concentrations show a coefficient correlation (r) of 0.63 and a normalized mean bias (NMB) of −37%. The low bias could be attributable to the underestimation of sulfate and OC; the simulated sulfate and OC concentrations have NMBs of −43% and −57%, respectively, while the NMBs for simulated nitrate, ammonium, and BC concentrations are only −15%, −5%, and −17%, respectively. The simulated low bias in sulfate concentrations could be partly explained by lower emissions of NH_3 and SO_2 under RCP4.5 than in current emission inventories [*Zhang et al.*, 2009; *Huang et al.*, 2012]. Moreover, several recent studies [e.g., *He et al.*, 2014; *X. Huang et al.*, 2014; *Y. Wang et al.*, 2014] have proposed some possible pathways for sulfate formation in China that are not fully considered in current models. The low biases in simulated OC

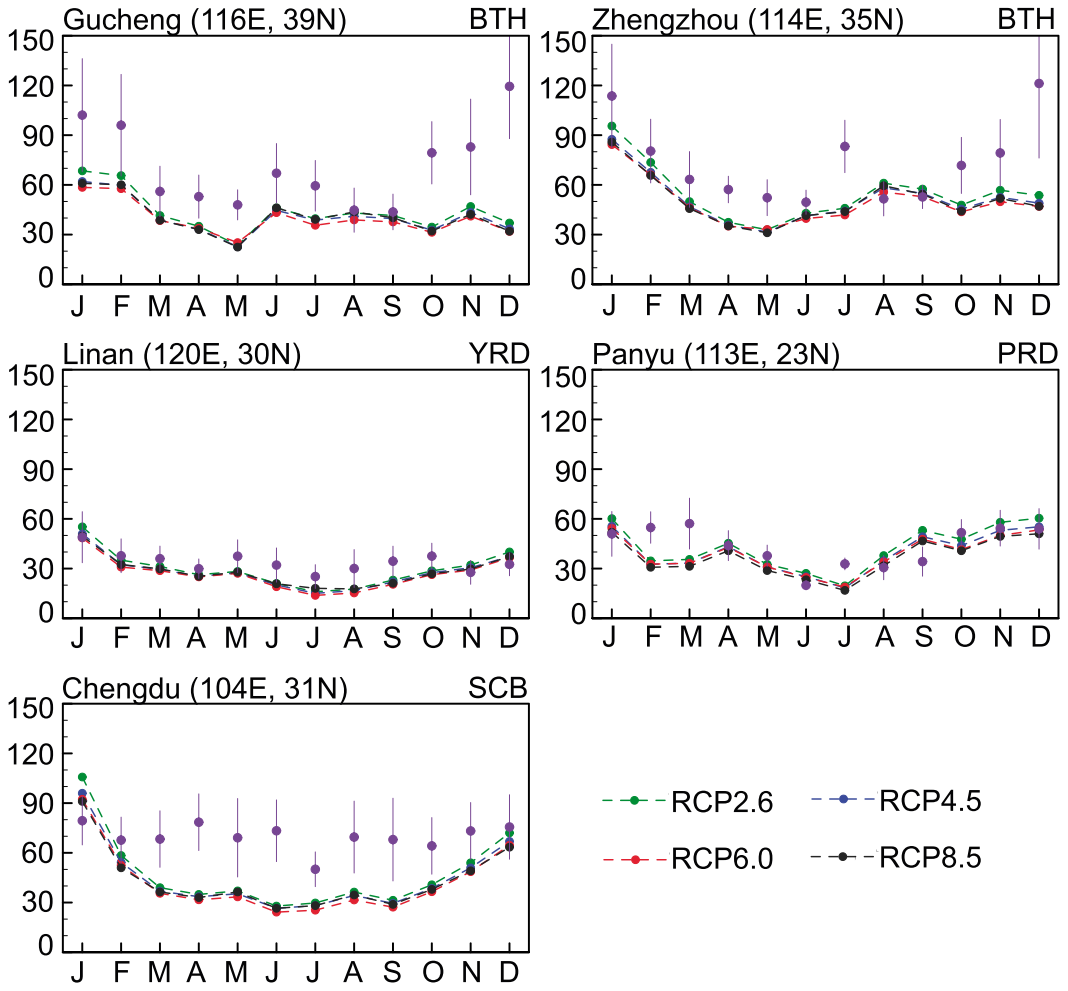

Figure 4. Comparison of simulated monthly mean concentrations (units: $\mu g\,m^{-3}$) of $PM_{2.5}$ for the year 2010 under RCP scenarios (different colored dashed lines) with actual measurements (purple dots) at five CAWNET sites. These five sites are all located in polluted regions (as indicated in the top-right corner of each panel, see Figure 3 for definitions).

could be attributable to underestimated OC emissions under RCP4.5 and the exclusion of SOA formation in our simulations.

We also compare our simulated changes (2000–2010) of $PM_{2.5}$ with the changes from two previous studies: one is a 15 year (1998–2012) global $PM_{2.5}$ concentration data set at a resolution of $1°\times1°$ derived from satellite-retrieved aerosol optical depth (AOD) products [*Boys et al.*, 2014], and the other is simulated $PM_{2.5}$ air quality over 1990–2010 across the Northern Hemisphere using the Weather Research and Forecasting-Community Multi-scale Air Quality model and historical emission inventories [*Xing et al.*, 2015]. Over 2000–2010, our simulated changes in $PM_{2.5}$ averaged over east China (20°–40°N, 100°–125°E) under the RCPs are 3.6–5.3 $\mu g\,m^{-3}$ (or 21–31%), which agree fairly well with the changes of $7.9\pm2.7\,\mu g\,m^{-3}$ from *Boys et al.* [2014] and 4.8 $\mu g\,m^{-3}$ (22%) from *Xing et al.* [2015]. Generally, the simulations with 2010 RCP emissions can reproduce the spatial distributions, seasonal variations, and historical changes of $PM_{2.5}$ level in China reasonably well.

4. Projected Changes in $PM_{2.5}$ Air Quality Over China Under RCP Scenarios

4.1. Future Changes in Annual Mean $PM_{2.5}$ Concentrations

Figure 6 shows the projected changes in annual mean $PM_{2.5}$ concentrations in 2010–2050 relative to 2000 over China. In the near term (2000–2030), the projected $PM_{2.5}$ under RCP2.6 holds at a high level during 2010–2020, with a maximum increase of 20 $\mu g\,m^{-3}$ in 2020 relative to 2000 over the NCP and SCB. By

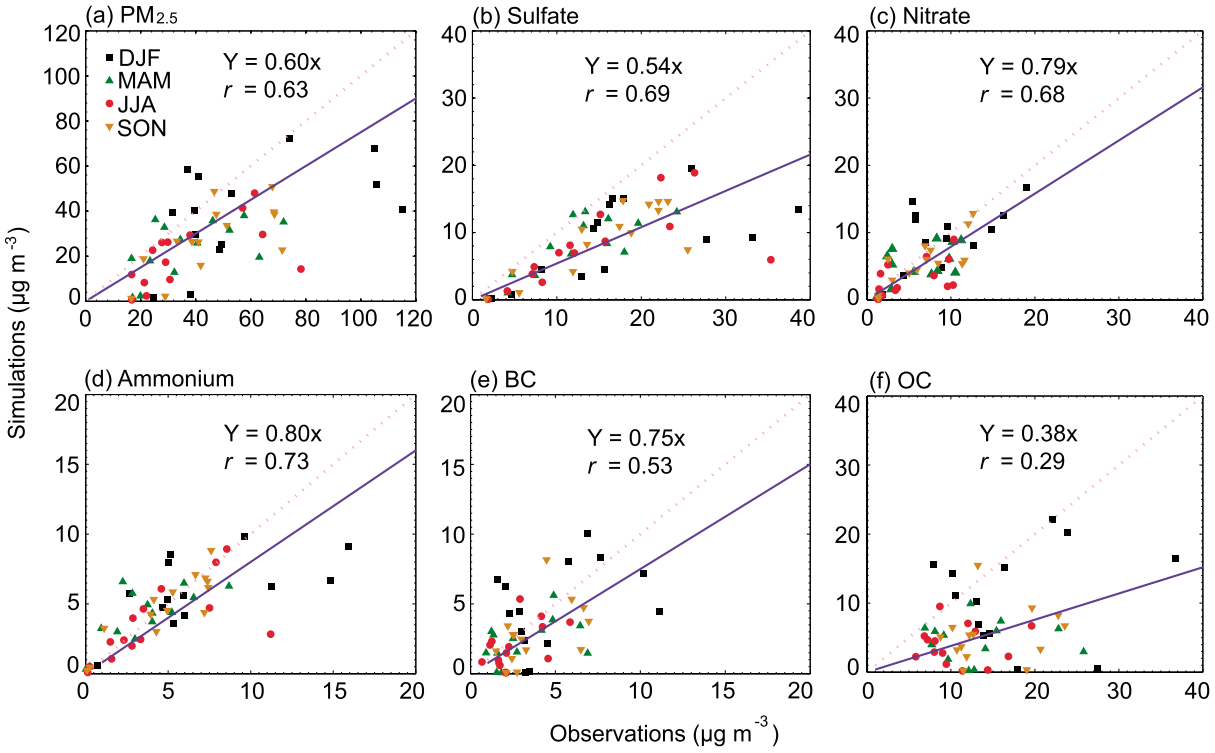

Figure 5. Comparison of observed and simulated seasonal mean concentrations (units: $\mu g\ m^{-3}$) of (a) $PM_{2.5}$ and its components: (b) sulfate, (c) nitrate, (d) ammonium, (e) BC, (f) OC at 14 CAWNET sites. The 1:1 (red dashed) line and linear fit (solid purple line and equation) are also shown in each plot. The *r* value is the correlation coefficient between observed and simulated concentrations. All of the *r* values shown above are statistically significant at the 95% level.

2030, increases in $PM_{2.5}$ concentrations are generally less than $5\ \mu g\ m^{-3}$ across China. The evolution and spatial distributions of projected $PM_{2.5}$ under RCP4.5 are similar to those under RCP2.6. Under RCP6.0, $PM_{2.5}$ concentrations demonstrate a rising trend during 2010–2030 and feature a large increase ($10–15\ \mu g\ m^{-3}$) over the NCP by 2030. Projected changes in $PM_{2.5}$ under RCP8.5 in 2010–2020 closely resemble those under RCP2.6. However, $PM_{2.5}$ concentrations under RCP8.5 could increase by $5–15\ \mu g\ m^{-3}$ over a large fraction of eastern China by 2030. Figure S2 shows the near-term changes in annual mean concentrations of $PM_{2.5}$ components. The largest changes are found in nitrate concentrations, which increase by $6–8\ \mu g\ m^{-3}$ over the SCB and NCP under RCP2.6, RCP6.0, and RCP8.5. Sulfate concentrations are projected to decrease (increase) by $2–4\ \mu g\ m^{-3}$ over the NCP (south China) under RCP2.6 (RCP8.5). Predicted OC concentrations in the near term decrease by $2–4\ \mu g\ m^{-3}$ over the NCP and SCB under RCP4.5, and changes in BC are generally within $\pm 2\ \mu g\ m^{-3}$ over China under all RCPs.

In the long term (2000–2050), large decreases of 15–20 (20–30) $\mu g\ m^{-3}$ in $PM_{2.5}$ concentrations under RCP2.6 (RCP4.5) are found over the NCP by 2050. Predicted $PM_{2.5}$ concentrations under RCP4.5 exhibit the lowest values, which mainly result from the low intensity of NH_3 and OC emissions under this scenario (see Figures 1c and 1e). High anthropogenic emissions under RCP6.0 contribute to the highest $PM_{2.5}$ concentrations among the RCPs, and the maximum increase ($20–30\ \mu g\ m^{-3}$) is predicted to occur over the NCP and SCB by 2040–2050. Under RCP8.5, projected $PM_{2.5}$ concentrations over China are comparable with those under RCP2.6. This can be explained by the fact that emissions of SO_2 and NO_x under RCP8.5 are larger by 121% and 55%, respectively, compared to those under RCP2.6, while NH_3 emissions under RCP8.5 are lower by 25%. Figure S3 shows the long-term changes in annual mean concentrations of $PM_{2.5}$ components. By 2050, the decrease in sulfate concentrations reaches $4–8\ \mu g\ m^{-3}$ over large areas of east China under all RCP scenarios except RCP6.0. Nitrate concentrations decrease by $4–8\ \mu g\ m^{-3}$ under RCP4.5 over the NCP, but increase over south China by $0–8\ \mu g\ m^{-3}$, under RCP2.6, RCP4.5, and RCP8.5. Decreases in ammonium and BC are small (less than $4\ \mu g\ m^{-3}$) in China under these three RCPs. OC concentrations decrease by $4–8\ \mu g\ m^{-3}$ over the NCP under all scenarios except RCP6.0.

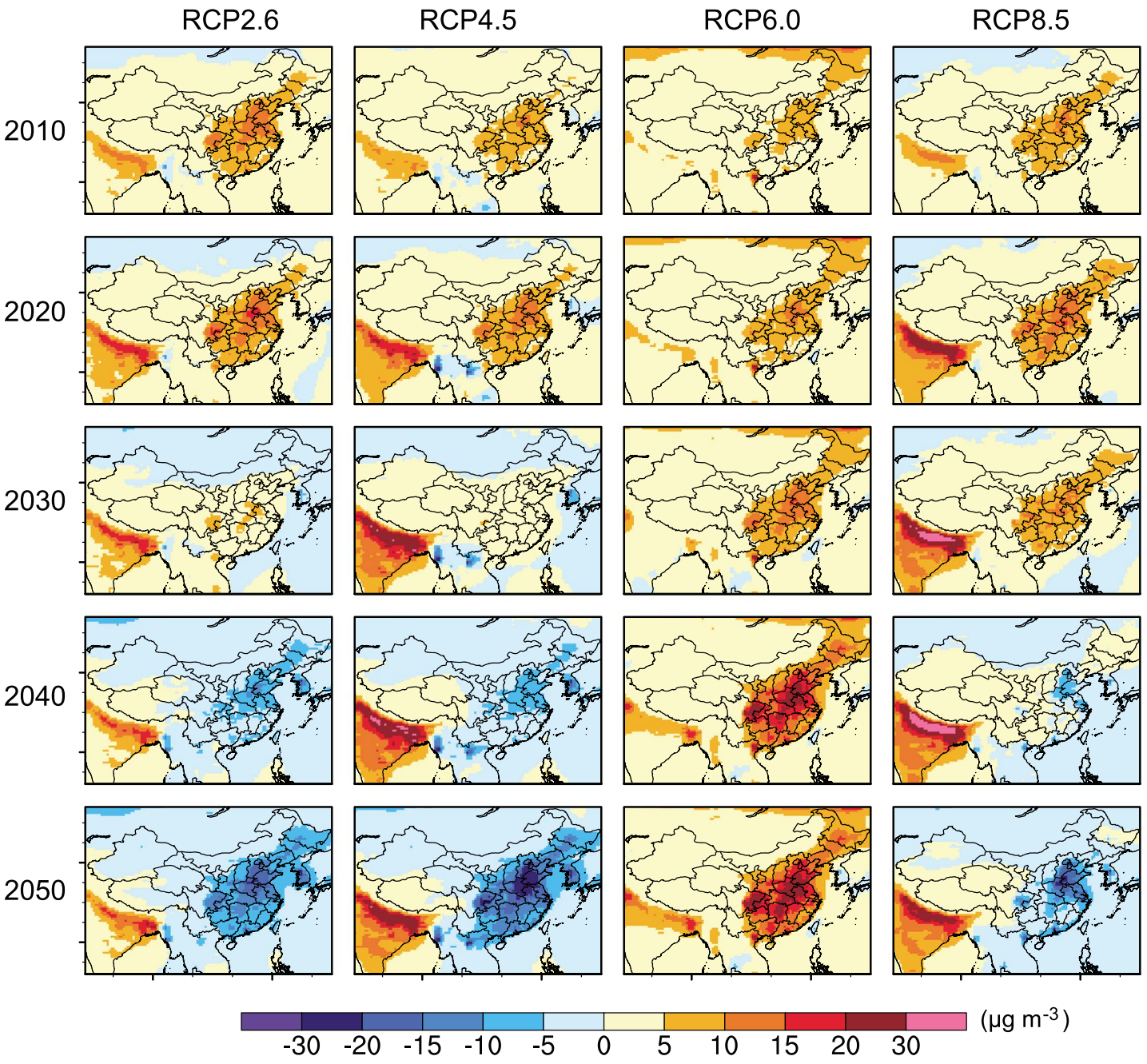

Figure 6. Projected changes in annual mean surface-layer $PM_{2.5}$ concentrations (units: $\mu g\ m^{-3}$) for the period 2010–2050 relative to 2000 under four RCP scenarios.

Based on the Atmospheric Chemistry and Climate Model Intercomparison Project multimodel outputs, *Silva et al.* [2016] concluded that population-weighted $PM_{2.5}$ concentrations over East Asia will decrease by 13, 15, and 12 $\mu g\ m^{-3}$ in 2050 relative to 2000 under RCP2.6, RCP4.5, and RCP8.5, respectively. Compared with the study of *Jiang et al.* [2013], who predicted a decrease in $PM_{2.5}$ of 1–8 $\mu g\ m^{-3}$ over east China in 2050 relative to 2000 under the SRES A1B scenario, the decreases (by 5–30 $\mu g\ m^{-3}$) in $PM_{2.5}$ concentrations over east China under RCP2.6, RCP4.5, and RCP8.5 in this study are quite significant. The large decreases in $PM_{2.5}$ concentrations in our simulations can be partly attributed to the differences in emission reductions between RCPs and A1B scenario and our higher model resolution that could better represent oxidant environment [*Zhang et al.*, 2011; *Yan et al.*, 2016] and transport processes [*Chen et al.*, 2009]. The projected changes in annual mean concentrations of $PM_{2.5}$ and their components under RCP2.6, RCP4.5, and RCP8.5 provide possible options

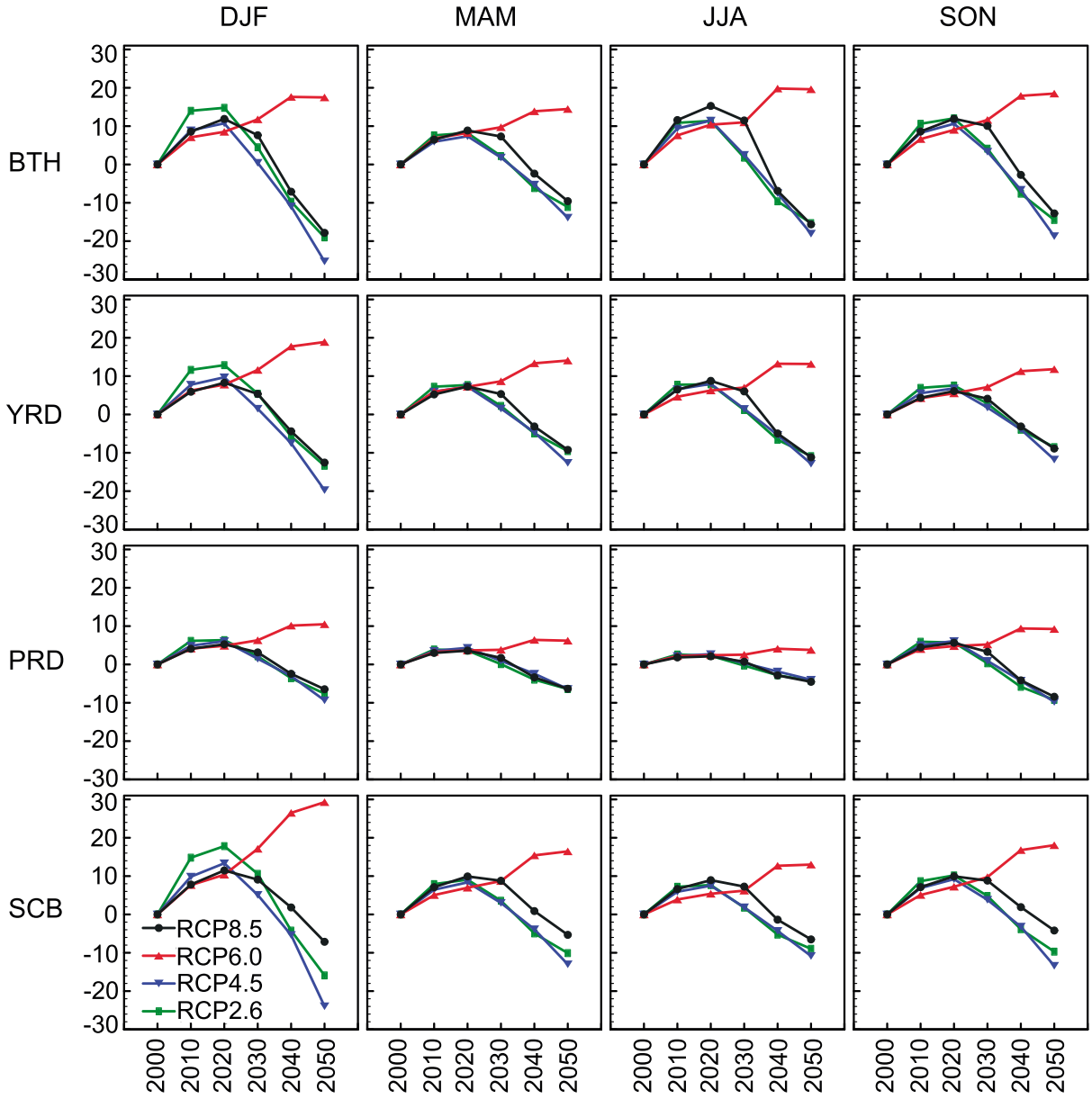

Figure 7. Projected changes in seasonal mean $PM_{2.5}$ levels (units: $\mu g\,m^{-3}$) for the period 2000–2050 over four polluted regions in China under four RCP scenarios.

to control and mitigate $PM_{2.5}$ air pollution on a national scale. In the following section, we pay particular attention to $PM_{2.5}$ air quality on the regional scale.

4.2. Future Changes in Seasonal Mean $PM_{2.5}$ Concentrations in Four Heavily Polluted Regions

The National Ambient Air Quality Standards (GB 3095-2012), launched by Ministry of Environmental Protection of China, will be implemented from 2016. The First Grand National Standard (FGNS) for annual $PM_{2.5}$ concentrations is no more than 35 $\mu g\,m^{-3}$. This standard is associated with a long-term mortality risk of around 15% higher relative to the air quality guidelines (10 $\mu g\,m^{-3}$) [*World Health Organization*, 2005]. Thus, we focus on the evolution of projected $PM_{2.5}$ levels over four heavily polluted regions (domains shown in Figure 3) in China: BTH (35°–40°N, 114°–120°E), Yangtze River Delta (YRD, 29.5°–32.5°N, 118°–122°E), Pearl River Delta (PRD, 21°–23.5°N, 112°–116°E), and SCB (28°–31.5°N, 102.5°–107.5°E). These four polluted regions are all urbanized, large city clusters, in which health concerns induced by $PM_{2.5}$ pollution make it urgent to take emission reduction measures. Figure 7 shows the projected future changes (2010–2050) of seasonal mean $PM_{2.5}$ concentrations relative to 2000 over the four regions under all the RCPs, and their maximum

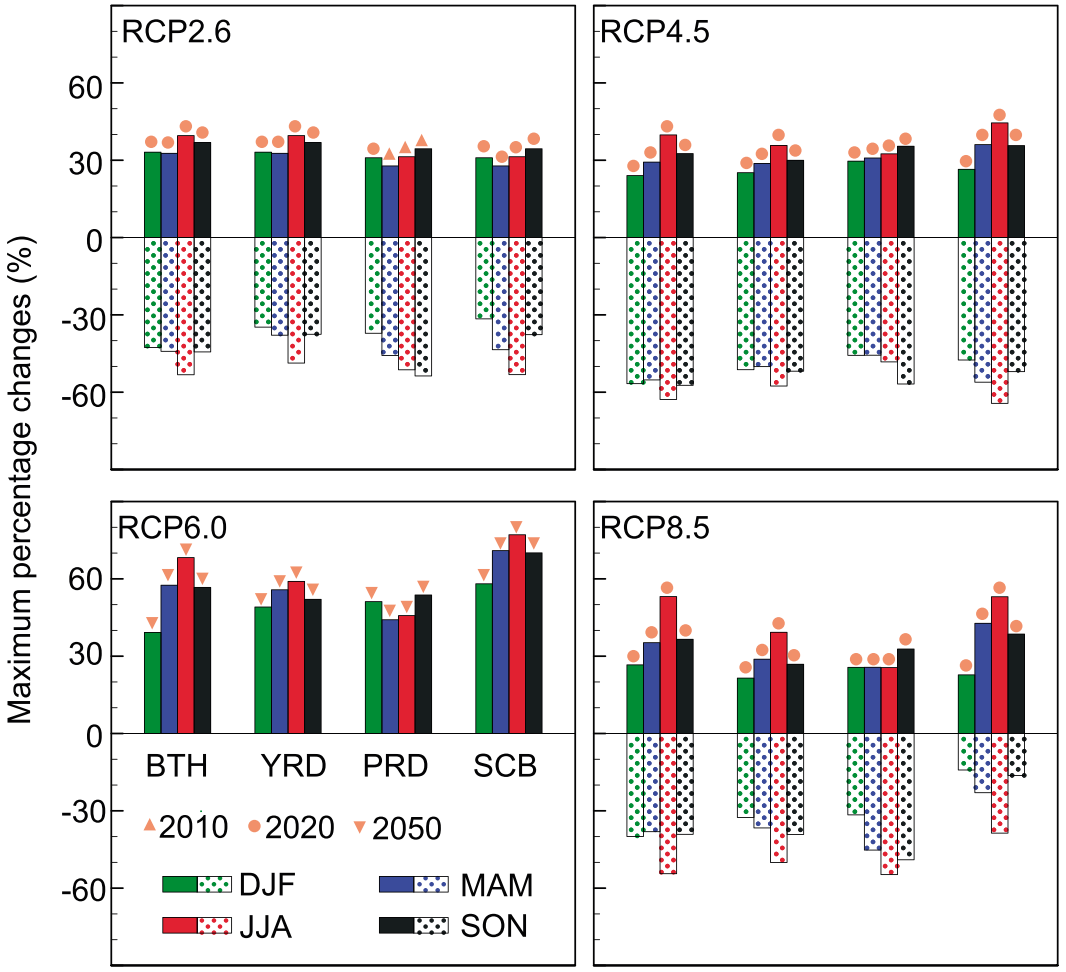

Figure 8. The maximum percentage changes (units: %) of projected seasonal mean $PM_{2.5}$ concentrations during 2010–2050 relative to 2000 over four polluted regions under four RCP scenarios. The maximum changes of increase (decrease) are shown as colored (dotted) columns. The years when the maximum increases occur are denoted by orange symbols, while the maximum decreases are all shown by 2050.

percentage changes are presented in Figure 8. We also show future evolutions (2000–2050) of $PM_{2.5}$ components over the four polluted regions in Figure 9.

4.2.1. BTH

Under the RCP scenarios, except RCP6.0, the largest increase in $PM_{2.5}$ concentration (~15 $\mu g\,m^{-3}$) is found by 2020, both in DJF under RCP2.6 and in JJA under RCP8.5, and their percentage changes relative to 2000 are +33% for DJF and +53% for JJA (Figure 8). The maximum decrease by 2050 is in DJF, with 19 $\mu g\,m^{-3}$ (−43%), 25 $\mu g\,m^{-3}$ (−57%), and 18 $\mu g\,m^{-3}$ (−40%) under RCP2.6, RCP4.5, and RCP8.5, respectively. In Figure 8, it can be seen that the largest percentage increases and decreases both occur in JJA under all RCPs, while the smallest changes are found in DJF. In terms of the FGNS, wintertime $PM_{2.5}$ concentrations that meet the FGNS will occur after 2040 under RCP2.6, RCP4.5, and RCP8.5, and summertime $PM_{2.5}$ concentrations will reach this goal by 2030 under RCP2.6 and RCP4.5.

We then show in Figure 9a the evolution of $PM_{2.5}$ components in DJF and JJA over BTH. Sulfate is the dominant aerosol species in JJA at present, but it is projected to decrease obviously after 2020 following changes in SO_2 emissions (Figure 1a). Nitrate concentrations hold high values during 2020–2040, even when NO_x emissions decrease (by 42–45%) during 2020–2040 under RCP2.6, RCP4.5, and RCP8.5. For example, the DJF nitrate concentrations for the year 2020 (2040) averaged over BTH are 18 (16), 16 (15), and 17 (19) $\mu g\,m^{-3}$ under RCP2.6, RCP4.5, and RCP8.5, respectively. High nitrate levels can be attributed to ammonium nitrate formation from both continuous increases in NH_3 emissions and reductions in sulfate concentrations [*Wang et al.*, 2013;

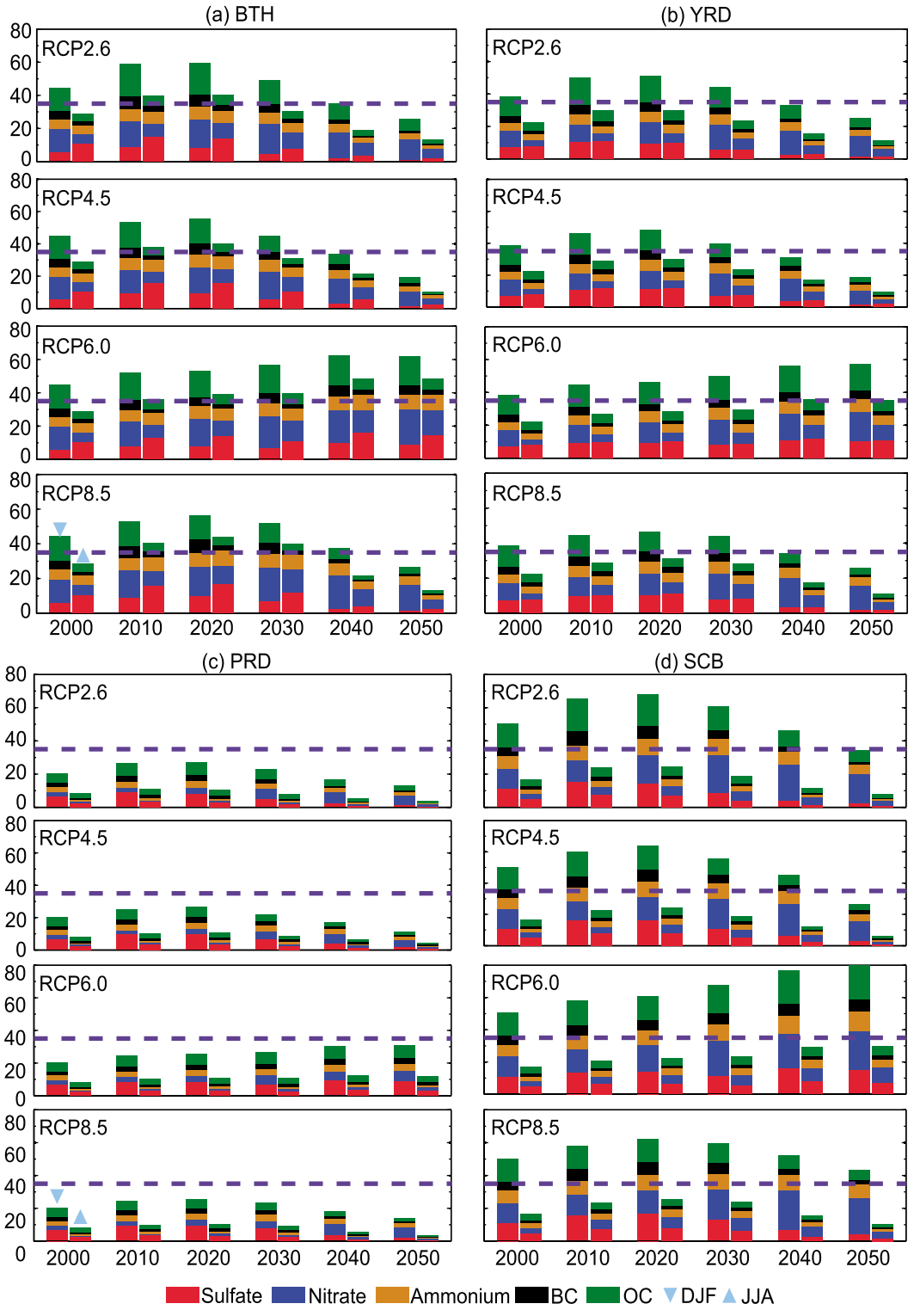

Figure 9. Projected (2000–2050) $PM_{2.5}$ component concentrations (units: $\mu g\ m^{-3}$) over (a) BTH, (b) YRD, (c) PRD, and (d) SCB, in (left column) DJF and (right column) JJA, under the different RCP scenarios. Also shown (by the dashed line) in each plot is the First Grand National Standard (less than 35 $\mu g\ m^{-3}$) for $PM_{2.5}$ concentrations.

Xing et al., 2015]. Future carbonaceous aerosols are considerably reduced, but OC in DJF by 2050 still accounts for 26%, 18%, and 15% of total $PM_{2.5}$ concentrations under RCP2.6, RCP4.5, and RCP8.5, respectively.

4.2.2. YRD

Among the RCP scenarios, except RCP6.0, the largest increase in $PM_{2.5}$ concentrations is ~13 $\mu g\,m^{-3}$ in DJF by 2020 under RCP2.6, and the maximum decrease (20 $\mu g\,m^{-3}$) is found in DJF by 2050 under RCP4.5. As for percentage changes, the maximum (minimum) values are +35% (−49%), +36% (−58%), and +39% (−50%) in JJA of 2020 (2050) under RCP2.6, RCP4.5, and RCP8.5, respectively. In consideration of the FGNS, future $PM_{2.5}$ levels in summer are expected to be controlled well, while winter $PM_{2.5}$ concentrations less than 35 $\mu g\,m^{-3}$ only appear after 2030. The evolutions of $PM_{2.5}$ components in YRD (Figure 9b) are very similar to those in BTH. With reduced sulfate concentrations in the future, the relative contribution of nitrate to $PM_{2.5}$ concentrations is expected to increase. Nitrate could account for 50% (38%), 47% (26%), and 53% (36%) of $PM_{2.5}$ concentrations in DJF (JJA) by 2050 under RCP2.6, RCP4.5, and RCP8.5, respectively, while its contribution to $PM_{2.5}$ in 2000 is only 25% (16%) in DJF (JJA). Following their emissions (Figures 1d and 1e), carbonaceous aerosols are projected to reduce considerably, with seasonal mean concentrations of 0.6–1.9 $\mu g\,m^{-3}$ for BC and 1.4–5.8 $\mu g\,m^{-3}$ for OC by 2050.

4.2.3. PRD

Future $PM_{2.5}$ concentrations in PRD are the lowest among the four polluted regions. The evolutions of $PM_{2.5}$ levels during 2000–2050 relative to 2000 are very similar to one another under the different RCPs, except RCP6.0. The largest increases in $PM_{2.5}$ concentrations are 5–6 $\mu g\,m^{-3}$ in DJF and SON by 2020, and the maximum decreases of 6–10 $\mu g\,m^{-3}$ by 2050 are also found in these two seasons. The largest percentage changes (increase or decrease) are found in SON (Figure 8). Projected $PM_{2.5}$ levels are under the FGSN, which do not exceed 5 $\mu g\,m^{-3}$ for JJA and 15 $\mu g\,m^{-3}$ for DJF by 2050. As for $PM_{2.5}$ components (Figure 9c), the largest difference in PRD compared with the other regions is that nitrate concentrations are doubled by 2050 relative to 2000, suggesting the importance of controlling nitrate over PRD in the future.

4.2.4. SCB

Under the different RCP scenarios, except RCP6.0, the largest increase in $PM_{2.5}$ concentration of ~18 (9) $\mu g\,m^{-3}$ is found by 2020 in DJF (JJA) under RCP2.6 (RCP8.5), and the percentage change relative to 2000 is +35% for DJF and +53% for JJA. The maximum decrease is simulated in DJF by 2050, by 16 $\mu g\,m^{-3}$ (32%), 24 $\mu g\,m^{-3}$ (48%), and 7 $\mu g\,m^{-3}$ (14%) under RCP2.6, RCP4.5, and RCP8.5, respectively. Compared with BTH, the control of future $PM_{2.5}$ pollution, especially in DJF, over SCB, is also challenging. In terms of the FGNS, $PM_{2.5}$ concentrations in winter less than 35 $\mu g\,m^{-3}$ are only shown under RCP2.6 and RCP4.5 by 2050, although summertime $PM_{2.5}$ is generally lower than 25 $\mu g\,m^{-3}$ during 2000–2050 under all RCPs, except RCP6.0. It should be noted that there is a low bias in our simulated summertime $PM_{2.5}$ concentrations when compared with the CAWNET observations. The evolutions of $PM_{2.5}$ components in SCB (Figure 9d) reflect those in BTH and YRD. Nitrate concentrations account for 48–51% of total $PM_{2.5}$ in DJF by 2050, and in JJA contributions from nitrate and OC to $PM_{2.5}$ are generally comparable under RCP2.6 and RCP4.5.

In summary, future $PM_{2.5}$ air quality over these polluted regions clearly improves under RCP2.6, RCP4.5, and RCP8.5. In consideration of the FGNS, however, controlling $PM_{2.5}$ pollution in BTH, YRD, and SCB will be challenging. Under both RCP2.6 and RCP4.5, wintertime (summertime) $PM_{2.5}$ in BTH that meets the FGNS is predicted to occur in 2040 (2030). In SCB (YRD) under these two scenarios, $PM_{2.5}$ concentrations in DJF below the FGNS are expected in 2050 (2040), while summertime $PM_{2.5}$ is well controlled. Under RCP8.5, wintertime (summertime) $PM_{2.5}$ in BTH that meets the FGNS will occur in 2050 (2040). In DJF and under RCP8.5, $PM_{2.5}$ concentrations reaching the FGNS are projected in 2040 in YRD, but the FGNS is never achieved in SCB. Future $PM_{2.5}$ air pollution will be worse if reduction measures are not taken timely, as RCP6.0 indicates. Note that natural aerosols and SOA were not considered in our projected $PM_{2.5}$ levels. Thus, if future $PM_{2.5}$ levels over BTH and SCB are expected to meet the FGNS, a conservative estimate is that it will take at least two decades to realize this goal, based on the RCP2.6, RCP4.5, and RCP8.5 scenarios.

5. Projected Evolutions of Aerosol DRF Over China Under the RCPs

5.1. Comparison of Simulated Aerosol Optical Depth With Observations

Figure 10 shows the simulated annual mean aerosol optical depth (AOD) for the year 2010 at 550 nm from the GEOS-Chem simulation driven by 2010 emissions under RCP4.5 and compares it with ground-based

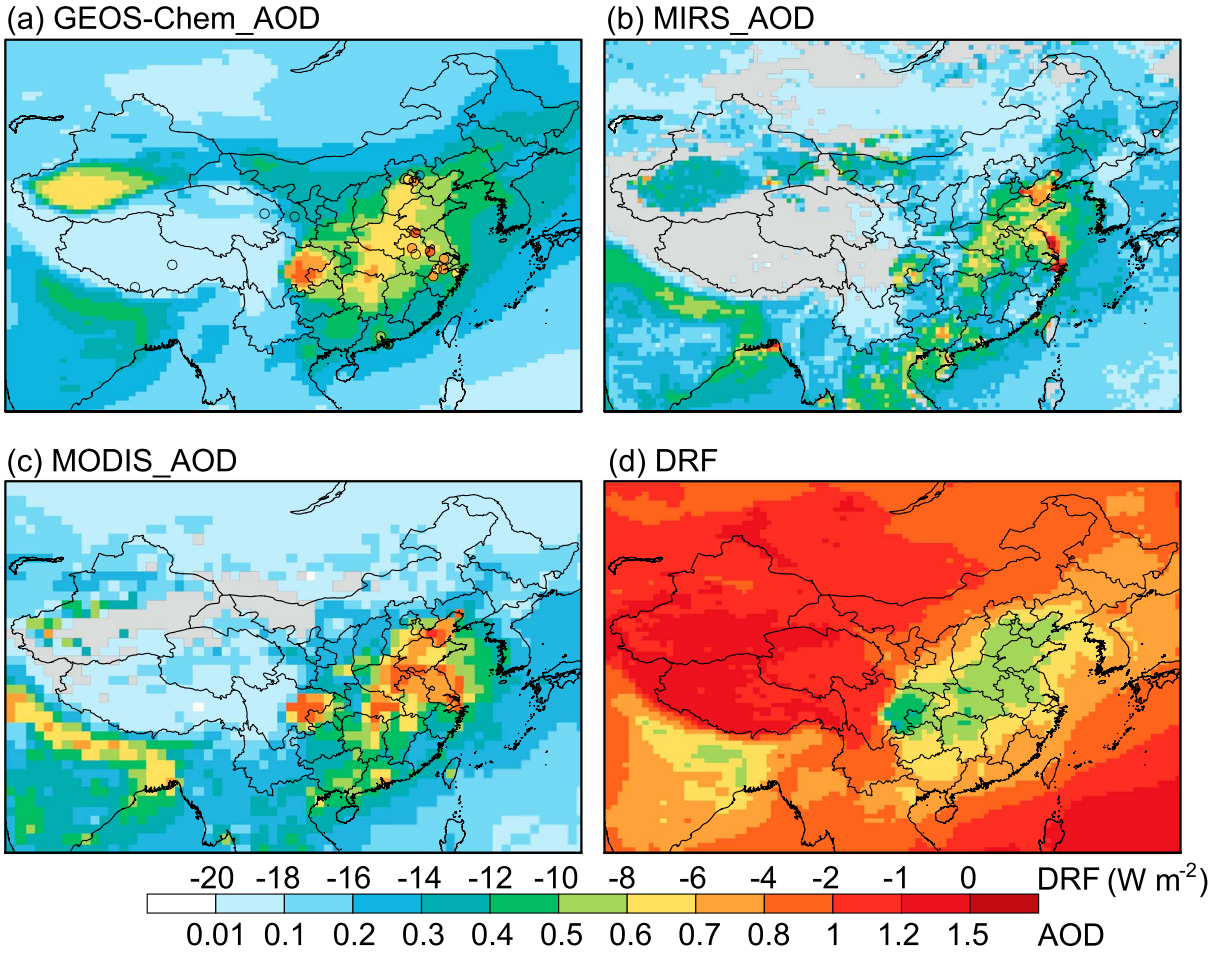

Figure 10. Annual mean (year 2010) AOD (colored scale bar, bottom) from (a) GEOS-Chem simulations for the year 2010 under RCP4.5 emissions at 550 nm, (b) MISR retrievals in the green band, and (c) MODIS retrievals at 550 nm. The grey indicates the missing data. The retrieved AOD (colored circles) at 550 nm for 20 sites from multiyear (2005–2014) AERONET observations is also shown in Figure 10a (see details in Table S2). (d) Simulated annual mean (year 2010) all-sky aerosol DRF (colored scale bar, top) (units: W m^{-2}) at the TOA under RCP4.5 emissions (DRF from natural aerosol is excluded because the meteorology is fixed at year 2010 simulations).

observations from the Aerosol Robotic Network (AERONET) [*Holben et al.*, 2001] and satellite retrievals from Microwave Integrated Retrieval System [*Martonchik et al.*, 1998] and MODIS (Moderate Resolution Imaging Spectroradiometer) [*Remer et al.*, 2005]. Simulated AOD includes both anthropogenic and natural aerosols (dust and sea salt). The AERONET AOD at 550 nm is obtained by logarithmically interpolating AOD between 440 nm and 675 nm from multiyear (2005–2014) averaged values at 20 sites in China (see details in Table S2). The Multiangle Imaging Spectroradiometer (MISR) AOD for the year 2010 is averaged over the monthly level-3 product (MIL3MAE4) in the green band (555 nm) with a resolution of 0.5°×0.5°, and the MODIS AOD for the year 2010 is based on the monthly level-3 product (MYD08_M3) from the Aqua satellite at 550 nm with a resolution of 1°×1°. The model results show high AODs of 0.8–1 over SCB and 0.6–0.7 over the NCP and south-central China (e.g., Hunan and Hubei provinces), and both of these ranges are consistent with the locations of high anthropogenic emissions and $PM_{2.5}$ concentrations. These three regions of high AOD can also be found in the AERONET AOD and satellite retrievals; however, the magnitude of AOD varies among these observations, with high AOD values of 0.8–1 from MODIS and 0.5–0.7 from MISR.

The comparisons of seasonal mean AOD between simulated and satellite retrieved values are shown in Figure S4. High AOD over SCB and eastern China in DJF and MAM seen by MODIS is well captured by the model. Simulated AOD over eastern China in JJA exhibits low bias in comparison with retrieved AOD. In SON, simulated and observed AODs are in good agreement over high-AOD regions. *Qi et al.* [2013] found that compared to AOD from AERONET sites in northern China, MODIS retrievals tend to overestimate AOD from

and MISR generally underestimates AOD. Our simulated AOD at the AERONET sites has a correlation coefficient (r) of 0.87 and a NMB of −22% (Table S2). Overall, the modeled magnitude and spatial distribution of AOD agree closely with observations.

5.2. Future Evolution of Aerosol DRF Over China

Figure 10d shows the simulated all-sky aerosol DRF for the year 2010 at the TOA under RCP4.5. A strong aerosol DRF of more than $-8\,W\,m^{-2}$ is apparent over SCB, NCP, and south-central China, which is consistent with the spatial distribution of AOD (Figure 10a). The simulated DRF averaged over east China (20°–45°N, 100°–125°E) is $-5.12\,W\,m^{-2}$, which is very similar to the annual mean DRF of total aerosols ($-5.11\,W\,m^{-2}$) in eastern China (21°–37°N, 110°–120°E) obtained by *Qian et al.* [2003]. The total aerosol DRF over eastern China was only $-2.40\,W\,m^{-2}$ in the simulation of *Chang and Liao* [2009], who excluded nitrate DRF in their calculation of total DRF.

The projected annual mean all-sky aerosol DRF at the TOA for the period 2010–2050 relative to 2000 over China is shown in Figure 11. In each panel's top-right corner, the regional values averaged over east China (20°–45°N, 100°–125°E) are shown. The negative DRF relative to 2000 averaged over east China peaks in 2020, with value of $-1.02\,W\,m^{-2}$ under RCP2.6, $-0.94\,W\,m^{-2}$ under RCP4.5, and $-1.10\,W\,m^{-2}$ under RCP8.5. By 2050, the positive DRF (relative to 2000) is the largest over east China under RCP2.6, RCP4.5, and RCP8.5, because emissions of aerosols and aerosol precursors (except NH_3 emissions) are considerably reduced by then (Figure 1). The aerosol DRF in 2050 relative to 2000 averaged over east China is a warming of $0.66\,W\,m^{-2}$ under RCP8.5 and of $1.88\,W\,m^{-2}$ under RCP4.5. As for RCP2.6, the value is $1.22\,W\,m^{-2}$, lying between the values of RCP4.5 and RCP8.5. High anthropogenic emissions under RCP6.0 result in a strongly negative DRF during 2000–2050, and the aerosol DRF over east China in 2050 relative to 2000 is $-2.73\,W\,m^{-2}$.

We also show, in Figure 12, the all-sky speciated aerosol DRF at the TOA for the period 2010–2050 over east China (as defined in Figure 11). Under RCP2.6, RCP4.5, and RCP8.5, the total aerosol DRF changes from approximately $-5\,W\,m^{-2}$ in 2010 to −3.6 to $-2.4\,W\,m^{-2}$ in 2050, which is mainly caused by less cooling of 1.7–1.9 $W\,m^{-2}$ from sulfate, less cooling of 0.4–0.7 $W\,m^{-2}$ from OC, and less cooling of 0.2–0.4 $W\,m^{-2}$ from ammonium in 2050 relative to 2010. The BC DRF shows an obvious decrease in warming of 0.4–0.7 $W\,m^{-2}$ from 2010 to 2050, but it counteracts the warming due to the decreases in concentrations of scattering aerosols [*Li et al.*, 2016]. The cooling by nitrate DRF is enhanced by 0.3–0.7 $W\,m^{-2}$ over east China from 2010 to 2050, and nitrate becomes the largest contributor to the total aerosol DRF after 2030. By 2050, the nitrate DRF over east China under RCP8.5 is $0.5\,W\,m^{-2}$ higher than that under RCP4.5. This indicates that about half of the difference in year 2050 aerosol DRF between RCP4.5 and RCP8.5 can be attributed to the difference in nitrate DRF.

The projected aerosol DRF in 2050 relative to 2000 averaged over eastern China is warming of 1.22, 1.88, and $0.66\,W\,m^{-2}$ under RCP2.6, RCP4.5, and RCP8.5, respectively. These changes are significant when compared to the global annual mean radiative forcing values by carbon dioxide ($+1.82\,W\,m^{-2}$) and tropospheric O_3 ($+0.40\,W\,m^{-2}$) [*IPCC*, 2013]. In addition, the increasing importance of nitrate DRF in total DRF in the future has also been reported by other studies [e.g., *Hauglustaine et al.*, 2014; *Li et al.*, 2015; *Paulot et al.*, 2016]. *Li et al.* [2015] concluded that nitrate will contribute to over 60% of the total aerosol DRF in East Asia by the end of this century. Furthermore, projected contributions of nitrate AOD to global total anthropogenic AOD are predicted to increase from a present-day value of 13% to 46–64% in 2100 under different RCPs [*Hauglustaine et al.*, 2014].

6. Implications for Mitigation Options

The evolution of projected $PM_{2.5}$ levels under different RCP scenarios has important implications for mitigation options of regional $PM_{2.5}$ pollution. According to the Paris Agreement contracted last year, there is a goal to keep the increase in global mean temperature below 2°C, relative to preindustrial levels, and an aim to limit the increase to 1.5°C. RCP2.6 and RCP4.5 are the two scenarios whose increases in temperature are likely not to exceed 1.5°C and 2°C, respectively [*IPCC*, 2013]. Over polluted regions in China, therefore, the expectation should be to achieve a decrease in $PM_{2.5}$ concentrations of 38–58% in 2050 relative to 2000, to adhere with the Paris Agreement. However, such emission reductions barely guarantee a 2050 $PM_{2.5}$ level below the FGNS over China as a whole.

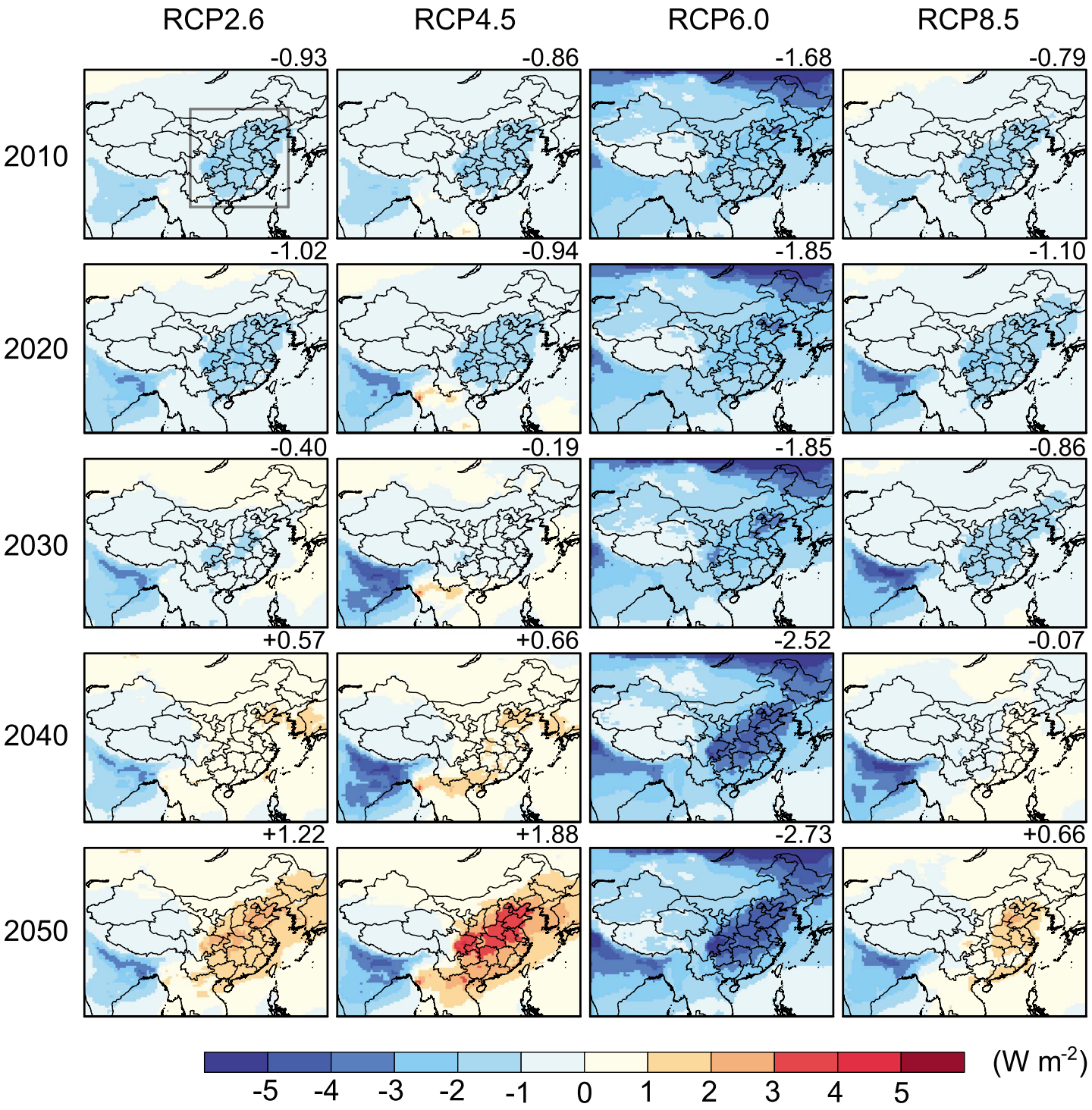

Figure 11. Projected changes in annual mean all-sky aerosol DRF (units: W m^{-2}) at the TOA in China for the period 2010–2050 relative to 2000 under different RCP scenarios. The DRF averaged over east China ((20°–45°N, 100°–125°E) as the grey rectangle in the first plot indicates) is shown in each panel's top-right corner.

The difficulty in controlling future $PM_{2.5}$ levels relates to the fact that concentrations of $PM_{2.5}$ components do not respond to reductions in their emissions in a simple linear fashion. The changes in concentrations of $PM_{2.5}$ components as well as the changes in emissions of aerosols and aerosol precursors in 2050 relative to 2000 are summarized in Table S3 for the four polluted regions under the four RCP scenarios. It can

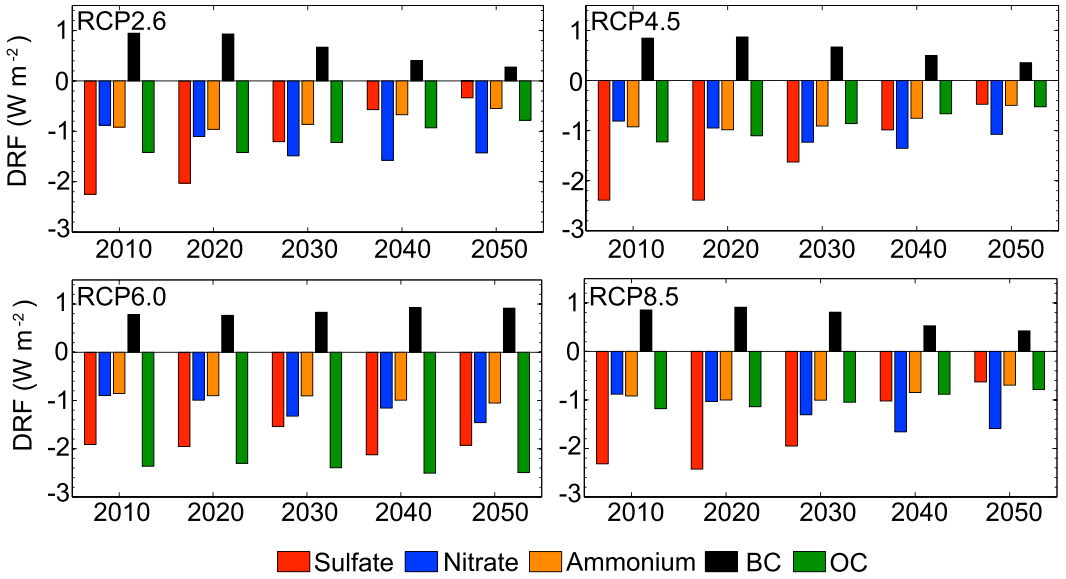

Figure 12. Projected annual mean all-sky speciated aerosol DRF (units: W m^{-2}) at the TOA for the period 2010–2050 averaged over east China ((20°–45°N, 100°–125°E) as defined in Figure 11) under RCPs.

be seen that changes in carbonaceous aerosols mainly follow their emissions, while changes of SNA aerosol depend largely on the change of SNA chemistry (as shown in Figure 13). Specifically, sulfate is expected to experience substantial reductions due to decreased SO_2 emissions. However, under RCP2.6, RCP4.5, and RCP8.5, the projected sulfate concentrations by 2050 are 1.0–2.5 μg m^{-3} in BTH, 1.5–2.3 μg m^{-3} in YRD, 0.6–2.3 μg m^{-3} in PRD, and 0.9–4.3 μg m^{-3} SCB, which are still comparable with present-day levels in the U.S. and Europe [*Xing et al.*, 2015]. Carbonaceous aerosols are also effectively reduced through decreased emissions; however, OC concentrations by 2050 still hold high values of 1.6–6.8 μg m^{-3} in BTH, 1.8–5.8 μg m^{-3} in YRD, 1.0–2.8 μg m^{-3} in PRD, and 1.5–6.9 μg m^{-3} in SCB, under RCP2.6, RCP4.5, and RCP8.5. Future nitrate concentrations are also projected to remain at relatively high levels. For example, nitrate concentrations in DJF over 2000–2050 in BTH are within 12–19, 9–17, and 14–19 μg m^{-3} under RCP2.6, RCP4.5, and RCP8.5, respectively.

To explore how future SNA aerosol formation is affected by emission changes under the different RCP scenarios, we chose two metrics (the calculations of these metrics are based on the units of mol m^{-3} for aerosol concentration and mol m^{-2} s^{-1} for emissions): (1) the degree of sulfate neutralization (DSN), estimating the neutralization of sulfate by ammonium ([*Pinder et al.*, 2008] DSN = $\left(\left[NH_4^+\right] - \left[NO_3^-\right]\right)/\left[SO_4^{2-}\right]$) and (2) the nitration ratio (NR) ([*Xing et al.*, 2015] NR = nitrate concentration/NO_x emission), representing the relative amount of oxidized-N emission that is eventually converted to nitrate aerosol—changes in NR could thus indicate the relative effectiveness of NO_x controls under given conditions. Figure 13 shows the evolution of changes in DSN and NR over BTH during 2000–2050. We can see that the rate of increase in $NO_x + 2 \times SO_2$ emissions is faster than that of NH_3 over BTH during 2000–2020 (Figure 13e), when DSN and NR show obvious declines. Over the period 2020–2040, a large increasing trend is found for both DSN and NR under all the RCPs except RCP6.0, though SO_2 and NO_x emissions are reduced substantially during this period. The high NR during 2020–2040 that can be attributed to that high fraction of NO_x is neutralized by NH_3, which mainly results from the decrease in sulfate ammonium formation and the increase in NH_3 emissions. This suggests an offset in the effectiveness of controlling $PM_{2.5}$ levels due to the increasing NH_3 emissions in this region. In addition, DSN and NR in JJA peak after 2040 over BTH under all RCPs except RCP6.0, while in DJF they show a continuous and faster increase up to 2050. This indicates that greater efforts should be taken with control measures of $PM_{2.5}$ in DJF. The importance of controlling NH_3 emissions should be carefully considered, because NH_3 plays a critical role in influencing the formation of SNA aerosol, and the projected speed of increase in NH_3 emissions in China over 2010–2050 is generally twice that at the global scale, except under RCP8.5 (Figure 13f).

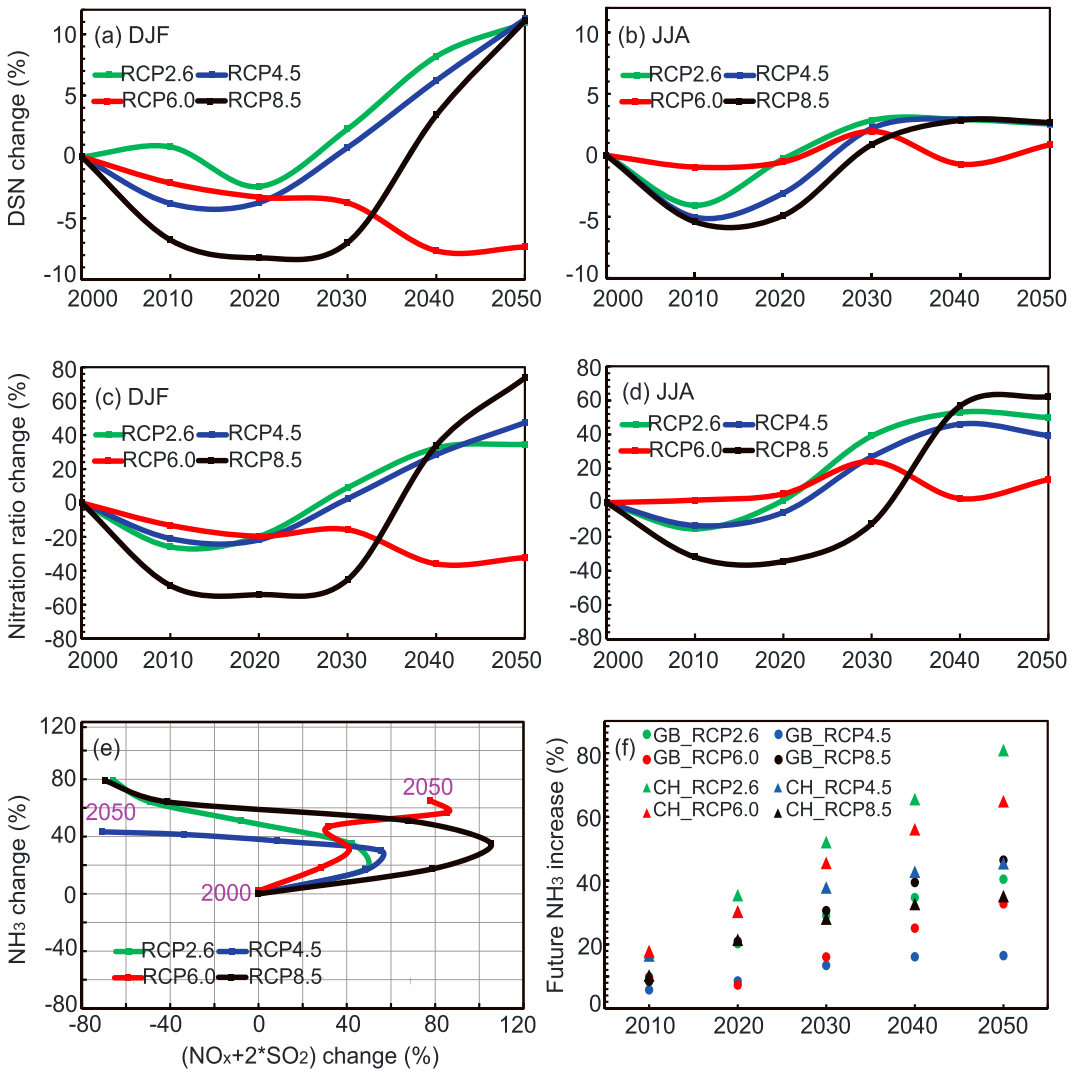

Figure 13. Evolution of SNA (sulfate-nitrate-ammonium) chemistry under RCPs over BTH (results are calculated based on the units of mol m^{-3} for aerosol concentrations and mol m^{-2} s^{-1} for emissions): (a and b) changes in DSN (degree of sulfate neutralization), (c and d) changes in NR (nitration ratio = (nitrate concentration/NO_x emission)), and (e) changes in NH_3 demand versus supply. $NO_x + 2 \times SO_2$ represents the amount of NH_3 needed for complete neutralization. (f) Increase (units: %) in NH_3 emissions during 2010–2050 relative to 2000 in China (triangles) and globally (circles), under the different RCP scenarios.

To improve air quality in the meantime, policymakers should consider the importance of DRF induced by decreased aerosols, which has been experienced in the U.S. [*Leibensperger et al.*, 2012] and Europe [*Turnock et al.*, 2016]. The warming effect of reducing aerosols for air quality improvement is significant. For example, $PM_{2.5}$ concentrations under RCP4.5 (RCP8.5) decrease by 49–58% (20–43%) over the four polluted regions in 2050 relative to 2000 (Table 1). The changes in aerosol concentrations lead to positive aerosol DRF values of 1.88 and 0.66 W m^{-2} over east China in 2050 relative to 2000 under RCP4.5 and RCP8.5, respectively. However, reducing BC can be taken as a win-win option for improving both air quality and mitigating near-term climate warming [*Shindell et al.*, 2012; *Li et al.*, 2016].

The *IPCC* [2013] has estimated that global mean surface temperature exhibited a warming by 0.85°C (0.65–1.06°C) from 1880 to 2012, and the related radiative forcing values in 2011 relative to 1750 by well-mixed greenhouse gases (CO_2, CH_4, N_2O, and halocarbons) and aerosols were +2.83 and −0.90 W m^{-2}, respectively. Thus, our predicted positive aerosol DRF values of 0.7–1.9 W m^{-2} over east China in 2050 relative to 2000 under the RCPs except RCP6.0 have important implications for regional climate.

Table 1. Changes in $PM_{2.5}$ Concentrations (Units: $\mu g\,m^{-3}$) Over Four Polluted Regions, and Changes in Aerosol DRF (Units: $W\,m^{-2}$) Over East China (20°–45°N, 100°–125°E) in 2050 Relative to 2000 Under the Different RCP Scenarios[a]

	Change in $PM_{2.5}$ ($\mu g\,m^{-3}$)				Change in DRF ($W\,m^{-2}$)
Scenario	BTH	YRD	PRD	SCB	East China
RCP2.6	−15.0 (−46%)	−10.6 (−39%)	−6.9 (−46%)	−11.2 (−38%)	+1.2 (+29%)
RCP4.5	−19.0 (−58%)	−14.3 (−53%)	−7.4 (−49%)	−15.3 (−53%)	+1.9 (+44%)
RCP6.0	+17.5 (+53%)	+14.5 (+54%)	+7.4 (+50%)	+19.2 (+66%)	−2.7 (−64%)
RCP8.5	−14.0 (−43%)	−10.5 (−39%)	−6.4 (−43%)	−5.8 (−20%)	+0.7 (+16%)

[a]Numbers in parentheses are the percentage changes.

7. Conclusions

This study applied the nested-grid version of GEOS-Chem model with high horizontal resolution (0.5° × 0.667°) to examine future changes (2000–2050) of projected $PM_{2.5}$ levels and associated aerosol DRF over China in response to emission changes under four RCP scenarios. The simulated current (year 2010) $PM_{2.5}$ concentrations reasonably captured the spatiotemporal distributions of observed values in China.

The model results show an improvement in future $PM_{2.5}$ air pollution. By 2050, the projected maximum decreases in $PM_{2.5}$ over east China are 15–30 $\mu g\,m^{-3}$, under RCP2.6, RCP4.5, and RCP8.5. However, the FGNS implemented in 2016 challenges the control of future $PM_{2.5}$ air pollution in China, especially over heavily polluted regions. In BTH (YRD), a wintertime $PM_{2.5}$ level meeting the FGNS only occurs after 2040 (2030). The first achievement of summertime $PM_{2.5}$ concentrations below the FGNS in BTH happens around 2030 under both RCP2.6 and RCP4.5. In SCB, the wintertime $PM_{2.5}$ level is highest among the four regions, and $PM_{2.5}$ concentrations less than 35 $\mu g\,m^{-3}$ only appear under RCP2.6 and RCP4.5, by 2050. Summertime $PM_{2.5}$ concentrations in SCB are always below 25 $\mu g\,m^{-3}$ for the period 2000–2050 under all RCPs except RCP6.0. $PM_{2.5}$ pollution in PRD is generally controlled well under RCP2.6, RCP4.5, and RCP8.5.

Concentrations of $PM_{2.5}$ components alter considerably under emission changes. Changes in sulfate follow decreases in SO_2 emissions, but sulfate concentrations by 2050 over China are still comparable with present-day levels in the U.S. and Europe. Nitrate remains at a high level, even showing a rapid increase, although NO_x emissions are reduced substantially (42–45%) during 2020–2040. NH_3 plays a critical role in modulating the formation of SNA aerosol, and the speed of increase in projected NH_3 emissions in China is twice that at the global scale. Carbonaceous aerosols show a large reduction, but the control of OC emissions needs to be stringent because the projected OC by 2050 is the second largest contributor to $PM_{2.5}$ concentrations.

The future annual mean aerosol DRF in 2050 relative to 2000 over east China (20°–45°N, 100°–125°E) is simulated to be warming of 1.22, 1.88, and 0.66 $W\,m^{-2}$ under RCP2.6, RCP4.5, and RCP8.5, respectively. Such warming effects of reduced aerosol are significant. When considering both health and climate effects of $PM_{2.5}$ over China, for example, $PM_{2.5}$ concentrations averaged over east China under RCP4.5 (RCP2.6) decrease by 54% (43%) in 2050 relative to 2000, but at the cost of the DRF warming by 1.88 (1.22) $W\,m^{-2}$. Moreover, reducing BC emissions can be taken as a win-win option for both air quality and climate warming.

Although projected future changes in $PM_{2.5}$ levels and corresponding DRFs under RCP scenarios provide us with important clues for mitigation efforts, uncertainties exist in such projections. For instance, the effects of future interannual to decadal time scale climate change on $PM_{2.5}$ levels [*Liao et al.*, 2006; *Zhu et al.*, 2012; *Mu and Liao*, 2014] were not considered in this study; plus, fully coupled chemistry-climate model estimates that combine the effects of future emissions and climate change on $PM_{2.5}$ air quality are further needed [*Raes et al.*, 2010; *Fiore et al.*, 2012]. Moreover, the prediction of $PM_{2.5}$ levels is also affected by mineral dust [*He et al.*, 2014; *X. Huang et al.*, 2014] and SOA chemistry in simulations [*Fu and Liao*, 2012; *R.-J. Huang et al.*, 2014], which are further issues that need to be addressed.

Acknowledgments
This work was supported by the National Basic Research Program of China (973 program, grant 2014CB441202), the Strategic Priority Research Program of the Chinese Academy of Sciences (grant XDA05100503), and the National Natural Science Foundation of China (grants 91544219, 41475137, and 41321064). Jonathan M. Moch acknowledges support from NSF GRFP (DGE1144152). We acknowledge the efforts of NASA's Goddard Earth Sciences Data and Information Services Center for providing satellite AOD products, the AERONET team for providing the AOD data sets, and the EDGAR team for providing the HTAP emission data sets used in our study. The GEOS-Chem model is managed by the Atmospheric Chemistry Modeling group at Harvard University, with support from NASA's ACMAP program. We thank three anonymous reviewers for their helpful comments. All of the observational data and model results have been archived by the corresponding author, Hong Liao (hongliao@nuist.edu.cn), and are available upon request.

References

Alexander, B., R. J. Park, D. J. Jacob, Q. B. Li, R. M. Yantosca, J. Savarino, C. C. W. Lee, and M. H. Thiemens (2005), Sulfate formation in sea-salt aerosols: Constraints from oxygen isotopes, *J. Geophys. Res.*, *110*, D10307, doi:10.1029/2004JD005659.

Bouwman, A. F., D. S. Lee, W. A. H. Asman, F. J. Dentener, K. W. Van Der Hoek, and J. G. J. Olivier (1997), A global high-resolution emission inventory for ammonia, *Global Biogeochem. Cycles*, *11*(4), 561–587, doi:10.1029/97GB02266.

Boys, B. L., et al. (2014), Fifteen-year global time series of satellite-derived fine particulate matter, *Environ. Sci. Technol.*, *48*(19), 11,109–11,118, doi:10.1021/es502113p.

Butler, T. M., Z. S. Stock, M. R. Russo, H. A. C. Denier van der Gon, and M. G. Lawrence (2012), Megacity ozone air quality under four alternative future scenarios, *Atmos. Chem. Phys.*, *12*(10), 4413–4428, doi:10.5194/acp-12-4413-2012.

Cao, J.-J., Z.-X. Shen, J. C. Chow, J. G. Watson, S.-C. Lee, X.-X. Tie, K.-F. Ho, G.-H. Wang, and Y.-M. Han (2012), Winter and summer PM2.5 chemical compositions in fourteen Chinese cities, *J. Air Waste Manage. Association*, *62*(10), 1214–1226, doi:10.1080/10962247.2012.701193.

Carmichael, G. R., et al. (2009), Asian aerosols: Current and tear 2030 distributions and implications to human health and regional climate change, *Environ. Sci. Technol.*, *43*(15), 5811–5817, doi:10.1021/es8036803.

Chang, W. Y., and H. Liao (2009), Anthropogenic direct radiative forcing of tropospheric ozone and aerosols from 1850 to 2000 estimated with IPCC AR5 emissions inventories, *Atmos. Oceanic Sci. Lett.*, *2*, 201–207.

Chen, D., Y. Wang, M. B. McElroy, K. He, R. M. Yantosca, and P. Le Sager (2009), Regional CO pollution and export in China simulated by the high-resolution nested-grid GEOS-Chem model, *Atmos. Chem. Phys.*, *9*(11), 3825–3839, doi:10.5194/acp-9-3825-2009.

Colette, A., et al. (2013), European atmosphere in 2050, a regional air quality and climate perspective under CMIP5 scenarios, *Atmos. Chem. Phys.*, *13*(15), 7451–7471, doi:10.5194/acp-13-7451-2013.

Fairlie, T. D., D. J. Jacob, and R. J. Park (2007), The impact of transpacific transport of mineral dust in the United States, *Atmos. Environ.*, *41*, 1251–1266, doi:10.1016/j.atmosenv.2006.09.048.

Fiore, A. M., et al. (2012), Global air quality and climate, *Chem. Soc. Rev.*, *41*(19), 6663–6683, doi:10.1039/C2CS35095E.

Fu, T. M., et al. (2012), Carbonaceous aerosols in China: Top-down constraints on primary sources and estimation of secondary contribution, *Atmos. Chem. Phys.*, *12*(5), 2725–2746, doi:10.5194/acp-12-2725-2012.

Fu, Y., and H. Liao (2012), Simulation of the interannual variations of biogenic emissions of volatile organic compounds in China: Impacts on tropospheric ozone and secondary organic aerosol, *Atmos. Environ.*, *59*(0), 170–185, doi:10.1016/j.atmosenv.2012.05.053.

Gao, M., S. K. Guttikunda, G. R. Carmichael, Y. Wang, Z. Liu, C. O. Stanier, P. E. Saide, and M. Yu (2015), Health impacts and economic losses assessment of the 2013 severe haze event in Beijing area, *Sci. Total Environ.*, *511*, 553–561, doi:10.1016/j.scitotenv.2015.01.005.

Gao, Y., C. Zhao, X. Liu, M. Zhang, and L. R. Leung (2014), WRF-Chem simulations of aerosols and anthropogenic aerosol radiative forcing in East Asia, *Atmos. Environ.*, *92*(0), 250–266, doi:10.1016/j.atmosenv.2014.04.038.

Guenther, A., T. Karl, P. Harley, C. Wiedinmyer, P. I. Palmer, and C. Geron (2006), Estimates of global terrestrial isoprene emissions using MEGAN (Model of Emissions of Gases and Aerosols from Nature), *Atmos. Chem. Phys.*, *6*(11), 3181–3210, doi:10.5194/acp-6-3181-2006.

Guo, S., et al. (2014), Elucidating severe urban haze formation in China, *Proc. Natl. Acad. Sci. U.S.A.*, *111*(49), 17,373–17,378, doi:10.1073/pnas.1419604111.

Hauglustaine, D. A., Y. Balkanski, and M. Schulz (2014), A global model simulation of present and future nitrate aerosols and their direct radiative forcing of climate, *Atmos. Chem. Phys.*, *14*(20), 11,031–11,063, doi:10.5194/acp-14-11031-2014.

He, H., Y. Wang, Q. Ma, J. Ma, B. Chu, D. Ji, G. Tang, C. Liu, H. Zhang, and J. Hao (2014), Mineral dust and NOx promote the conversion of SO2 to sulfate in heavy pollution days, *Sci. Rep.*, *4*, doi:10.1038/srep04172.

Heald, C. L., D. A. Ridley, J. H. Kroll, S. R. H. Barrett, K. E. Cady-Pereira, M. J. Alvarado, and C. D. Holmes (2014), Contrasting the direct radiative effect and direct radiative forcing of aerosols, *Atmos. Chem. Phys.*, *14*(11), 5513–5527, doi:10.5194/acp-14-5513-2014.

Holben, B. N., et al. (2001), An emerging ground-based aerosol climatology: Aerosol optical depth from AERONET, *J. Geophys. Res.*, *106*(D11), 12,067–12,097, doi:10.1029/2001JD900014.

Horton, D. E., C. B. Skinner, D. Singh, and N. S. Diffenbaugh (2014), Occurrence and persistence of future atmospheirc stagation events, *Nature Clim. Change* , *4*(8), 698–703, doi:10.1038/nclimate2272.

Huang, R.-J., et al. (2014), High secondary aerosol contribution to particulate pollution during haze events in China, *Nature*, *514*(7521), 218–222, doi:10.1038/nature13774.

Huang, X., Y. Song, M. Li, J. Li, Q. Huo, X. Cai, T. Zhu, M. Hu, and H. Zhang (2012), A high-resolution ammonia emission inventory in China, *Global Biogeochem. Cy.*, *26*(1), GB1030, doi:10.1029/2011GB004161.

Huang, X., Y. Song, C. Zhao, M. Li, T. Zhu, Q. Zhang, and X. Zhang (2014), Pathways of sulfate enhancement by natural and anthropogenic mineral aerosols in China, *J. Geophys. Res. Atmos.*, *119*, 14,165–14,179, doi:10.1002/2014JD022301.

Huang, X., Y. Song, C. Zhao, X. Cai, H. Zhang, and T. Zhu (2015), Direct radiative effect by multicomponent aerosol over China, *J. Clim.*, *28*(9), 3472–3495, doi:10.1175/JCLI-D-14-00365.1.

Intergovernmental Panel on Climate Change (IPCC), Climate Change (2013), *The Physical Science Basis. Contribution of Working Group I to the Fifth Assessment Report of the Intergovernmental Panel on Climate Change*, Cambridge Univ. Press, Cambridge, U. K. and New York.

Jacob, D. J., and D. A. Winner (2009), Effect of climate change on air quality, *Atmos. Environ.*, *43*(1), 51–63, doi:10.1016/j.atmosenv.2008.09.051.

Janssens-Maenhout, G., M. Crippa, D. Guizzardi, and Z. Klimont (2015), HTAP_v2: A mosaic of regional and global emission grid maps for 2008 and 2010 to study hemispheric transport of air pollution, *Atmos. Chem. Phys.*, *15*(19), 11,411–11,432, doi:10.5194/acp-15-11411-2015.

Jiang, H., H. Liao, H. O. T. Pye, S. Wu, L. J. Mickley, J. H. Seinfeld, and X. Y. Zhang (2013), Projected effect of 2000–2050 changes in climate and emissions on aerosol levels in China and associated transboundary transport, *Atmos. Chem. Phys.*, *13*(16), 7937–7960, doi:10.5194/acp-13-7937-2013.

Jiang, J. K., W. Zhou, Z. Cheng, S. X. Wang, K. B. He, and J. M. Hao (2015), Particulate matter distributions in China during a winter period with frequent pollution episodes (January 2013), *Aerosol Air Qual. Res.*, *15*(2), 494–503, doi:10.4209/aaqr.2014.04.0070.

Kelly, J., P. A. Makar, and D. A. Plummer (2012), Projections of mid-century summer air-quality for North America: Effects of changes in climate and precursor emissions, *Atmos. Chem. Phys.*, *12*(12), 5367–5390, doi:10.5194/acp-12-5367-2012.

Kelly, F. J., and T. Zhu (2016), Transport solutions for cleaner air, *Science*, *352*(6288), 934–936, doi:10.1126/science.aaf3420.

Kirtman, B., S. B. Power, J. A. Adedoyin, G. J. Boer, R. Bojariu, I. Camilloni, F. J. Doblas-Reyes, A. M. Fiore, M. Kimoto, and G. A. Meehl (2013), Near-term climate change: Projections and predictability, in *Climate Change 2013: The Physical Science Basis (Chapter 11)*, edited by Contribution of Working Group I to the Fifth Assessment Report of the Intergovernmental Panel on Climate Change, Cambridge Univ. Press, Cambridge, U. K. and New York.

Lam, Y. F., J. S. Fu, S. Wu, and L. J. Mickley (2011), Impacts of future climate change and effects of biogenic emissions on surface ozone and particulate matter concentrations in the United States, *Atmos. Chem. Phys.*, *11*(10), 4789–4806, doi:10.5194/acp-11-4789-2011.

Lapina, K., D. K. Henze, J. B. Milford, C. Cuvelier, and M. Seltzer (2015), Implications of RCP emissions for future changes in vegetative exposure to ozone in the western U.S., *Geophys. Res. Lett.*, *42*, 4190–4198, doi:10.1002/2015GL063529.

Leibensperger, E. M., L. J. Mickley, D. J. Jacob, W. T. Chen, J. H. Seinfeld, A. Nenes, P. J. Adams, D. G. Streets, N. Kumar, and D. Rind (2012), Climatic effects of 1950–2050 changes in US anthropogenic aerosols—Part 2: Climate response, *Atmos. Chem. Phys.*, *12*(7), 3349–3362, doi:10.5194/acp-12-3349-2012.

Lelieveld, J., J. S. Evans, M. Fnais, D. Giannadaki, and A. Pozzer (2015), The contribution of outdoor air pollution sources to premature mortality on a global scale, *Nature*, *525*(7569), 367–371, doi:10.1038/nature15371.
Li, J., W.-C. Wang, Z. Sun, G. Wu, H. Liao, Y. Liu, and Q. Bao (2014), Decadal variation of East Asian radiative forcing due to anthropogenic aerosols during 1850–2100 and the role of atmospheric moisture, *Clim. Res.*, *61*, 241–257, doi:10.3354/cr01236.
Li, J., W.-C. Wang, H. Liao, and W. Y. Chang (2015), Past and futue direct radiative forcing of nitrate aerosol in East Asia, *Thero. Appl. Climatol.*, *121*(3), 445–458, doi:10.1007/s00704-014-1249-1.
Li, K., H. Liao, Y. Mao, and D. A. Ridley (2016), Source sector and region contributions to concentration and direct radiative forcing of black carbon in China, *Atmos. Environ.*, *124*, 351–366, doi:10.1016/j.atmosenv.2015.06.014.
Liao, H., W.-T. Chen, and J. H. Seinfeld (2006), Role of climate change in global predictions of future tropospheric ozone and aerosols, *J. Geophys. Res.*, *111*, D12304, doi:10.1029/2005JD006852.
Liao, H., W. Chang, and Y. Yang (2015), Climatic effects of air pollutants over china: A review, *Adv. in Atmos. Sci.*, *32*(1), 115–139, doi:10.1007/s00376-014-0013-x.
Liu, H., D. J. Jacob, I. Bey, and R. M. Yantosca (2001), Constraints from 210Pb and 7Be on wet deposition and transport in a global three-dimensional chemical tracer model driven by assimilated meteorological fields, *J. Geophys. Res.*, *106*(D11), 12,109–12,128, doi:10.1029/2000JD900839.
Lou, S., H. Liao, and B. Zhu (2014), Impacts of aerosols on surface-layer ozone concentrations in China through heterogeneous reactions and changes in photolysis rates, *Atmos. Environ.*, *85*(0), 123–138, doi:10.1016/j.atmosenv.2013.12.004.
Lu, Z., Q. Zhang, and D. G. Streets (2011), Sulfur dioxide and primary carbonaceous aerosol emissions in China and India, 1996–2010, *Atmos. Chem. Phys.*, *11*(18), 9839–9864, doi:10.5194/acp-11-9839-2011.
Mao, Y. H., H. Liao, Y. M. Han, and J. J. Cao (2016), Impacts of meteorological parameters and emissions on decadal and interannual variations of black carbon in China for 1980–2010, *J. Geophys. Res. Atmos.*, *121*, 1822–1843, doi:10.1002/2015JD024019.
Martonchik, J. V., D. J. Diner, R. A. Kahn, T. P. Ackerman, M. M. Verstraete, B. Pinty, and H. R. Gordon (1998), Techniques for the retrieval of aerosol properties over land and ocean using multiangle imaging, *IEEE Trans. Geosci. Remote Sens.*, *36*(4), 1212–1227, doi:10.1109/36.701027.
Mu, Q., and H. Liao (2014), Simulation of the interannual variations of aerosols in China: Role of variations in meteorological parameters, *Atmos. Chem. Phys.*, *14*(18), 9597–9612, doi:10.5194/acp-14-9597-2014.
Murray, L. T., D. J. Jacob, J. A. Logan, R. C. Hudman, and W. J. Koshak (2012), Optimized regional and interannual variability of lightning in a global chemical transport model constrained by LIS/OTD satellite data, *J. Geophys. Res.*, *117*, D20307, doi:10.1029/2012JD017934.
Park, R. J., D. J. Jacob, M. Chin, and R. V. Martin (2003), Sources of carbonaceous aerosols over the United States and implications for natural visibility, *J. Geophys. Res.*, *108*(D12), 4355, doi:10.1029/2002JD003190.
Park, R. J., D. J. Jacob, B. D. Field, R. M. Yantosca, and M. Chin (2004), Natural and transboundary pollution influences on sulfate-nitrate-ammonium aerosols in the United States: Implications for policy, *J. Geophys. Res.*, *109*, D15204, doi:10.1029/2003JD004473.
Paulot, F., D. J. Jacob, R. W. Pinder, J. O. Bash, K. Travis, and D. K. Henze (2014), Ammonia emissions in the United States, European Union, and China derived by high-resolution inversion of ammonium wet deposition data: Interpretation with a new agricultural emissions inventory (MASAGE_NH3), *J. Geophys. Res. Atmos.*, *119*, 4343–4364, doi:10.1002/2013JD021130.
Paulot, F., P. Ginoux, W. F. Cooke, L. J. Donner, S. Fan, M.-Y. Lin, J. Mao, V. Naik, and L. W. Horowitz (2016), Sensitivity of nitrate aerosols to ammonia emissions and to nitrate chemistry: Implications for present and future nitrate optical depth, *Atmos. Chem. Phys.*, *16*(3), 1459–1477, doi:10.5194/acp-16-1459-2016.
Pinder, R. W., R. L. Dennis, and P. V. Bhave (2008), Observable indicators of the sensitivity of PM2.5 nitrate to emission reductions—Part I: Derivation of the adjusted gas ratio and applicability at regulatory-relevant time scales, *Atmos. Environ.*, *42*(6), 1275–1286, doi:10.1016/j.atmosenv.2007.10.039.
Pye, H. O. T., H. Liao, S. Wu, L. J. Mickley, D. J. Jacob, D. K. Henze, and J. H. Seinfeld (2009), Effect of changes in climate and emissions on future sulfate-nitrate-ammonium aerosol levels in the United States, *J. Geophys. Res.*, *114*, D01205, doi:10.1029/2008JD010701.
Qi, Y., J. Ge, and J. Huang (2013), Spatial and temporal distribution of MODIS and MISR aerosol optical depth over northern China and comparison with AERONET, *Chinese Sci. Bull.*, *58*(20), 2497–2506, doi:10.1007/s11434-013-5678-5.
Qian, Y., L. R. Leung, S. J. Ghan, and F. Giorgi (2003), Regional climate effects of aerosols over China: Modeling and observation, *Tellus*, *55B*, 914–934, doi:10.1046/j.1435-6935.2003.00070.x.
Qu, W. J., R. Arimoto, X. Y. Zhang, C. H. Zhao, Y. Q. Wang, L. F. Sheng, and G. Fu (2010), Spatial distribution and interannual variation of surface PM10 concentrations over eighty-six Chinese cities, *Atmos. Chem. Phys.*, *10*(12), 5641–5662, doi:10.5194/acp-10-5641-2010.
Raes, F., H. Liao, W.-T. Chen, and J. H. Seinfeld (2010), Atmospheric chemistry-climate feedbacks, *J. Geophys. Res.*, *115*, D12121, doi:10.1029/2009JD013300.
Rattanavaraha, W., et al. (2016), Assessing the impact of anthropogenic pollution on isoprene-derived secondary organic aerosol formation in PM2.5 collected from the Birmingham, Alabama, ground site during the 2013 Southern Oxidant and Aerosol Study, *Atmos. Chem. Phys.*, *16*(8), 4897–4914, doi:10.5194/acp-16-4897-2016.
Remer, L. A., et al. (2005), The MODIS aerosol algorithm, products, and validation, *J. Atmos. Sci.*, *62*(4), 947–973, doi:10.1175/JAS3385.1.
Sauvage, B., R. V. Martin, A. van Donkelaar, X. Liu, K. Chance, L. Jaeglé, P. I. Palmer, S. Wu, and T. M. Fu (2007), Remote sensed and in situ constraints on processes affecting tropical tropospheric ozone, *Atmos. Chem. Phys.*, *7*(3), 815–838, doi:10.5194/acp-7-815-2007.
Shilling, J. E., et al. (2013), Enhanced SOA formation from mixed anthropogenic and biogenic emissions during the CARES campaign, *Atmos. Chem. Phys.*, *13*(4), 2091–2113, doi:10.5194/acp-13-2091-2013.
Shindell, D., et al. (2012), Simultaneously mitigating near-term climate change and improving human health and food security, *Science*, *335*(6065), 183–189, doi:10.1126/science.1210026.
Silva, R. A., et al. (2016), The effect of future ambient air pollution on human premature mortality to 2100 using output from the ACCMIP model ensemble, *Atmos. Chem. Phys. Discuss.*, *1–24*, doi:10.5194/acp-2015-1002.
Tagaris, E., K. Manomaiphiboon, K.-J. Liao, L. R. Leung, J.-H. Woo, S. He, P. Amar, and A. G. Russell (2007), Impacts of global climate change and emissions on regional ozone and fine particulate matter concentrations over the United States, *J. Geophys. Res.*, *112*, D14312, doi:10.1029/2006JD008262.
Trail, M., A. P. Tsimpidi, P. Liu, K. Tsigaridis, J. Rudokas, P. Miller, A. Nenes, Y. Hu, and A. G. Russell (2014), Sensitivity of air quality to potential future climate change and emissions in the United States and major cities, *Atmos. Environ.*, *94*(0), 552–563, doi:10.1016/j.atmosenv.2014.05.079.
Turnock, S. T., et al. (2016), The impact of European legislative and technology measures to reduce air pollutants on air quality, human health and climate, *Environ. Res. Lett.*, *11*(2), 024010, doi:10.1088/1748-9326/11/2/024010.
Val Martin, M., C. L. Heald, J. F. Lamarque, S. Tilmes, L. K. Emmons, and B. A. Schichtel (2015), How emissions, climate, and land use change will impact mid-century air quality over the United States: A focus on effects at national parks, *Atmos. Chem. Phys.*, *15*(5), 2805–2823, doi:10.5194/acp-15-2805-2015.

van Vuuren, D., et al. (2011), The representative concentration pathways: An overview, *Clim. Change*, *109*(1–2), 5–31, doi:10.1007/s10584-011-0148-z.

Wang, K., R. E. Dickinson, and S. Liang (2009), Clear sky visibility has decreased over land globally from 1973 to 2007, *Science*, *323*(5920), 1468–1470, doi:10.1126/science.1167549.

Wang, L. T., Z. Wei, J. Yang, Y. Zhang, F. F. Zhang, J. Su, C. C. Meng, and Q. Zhang (2014), The 2013 severe haze over southern Hebei, China: Model evaluation, source apportionment, and policy implications, *Atmos. Chem. Phys.*, *14*(6), 3151–3173, doi:10.5194/acp-14-3151-2014.

Wang, L., Y. Zhang, K. Wang, B. Zheng, Q. Zhang, and W. Wei (2016), Application of Weather Research and Forecasting Model with Chemistry (WRF/Chem) over northern China: Sensitivity study, comparative evaluation, and policy implications, *Atmos. Environ.*, *124*(B), doi:10.1016/j.atmosenv.2014.12.052.

Wang, S., and J. Hao (2012), Air quality management in China: Issues, challenges, and options, *J. Environ. Sci.*, *24*(1), 2–13, doi:10.1016/S1001-0742(11)60724-9.

Wang, Y., Q. Q. Zhang, K. He, Q. Zhang, and L. Chai (2013), Sulfate-nitrate-ammonium aerosols over China: Response to 2000–2015 emission changes of sulfur dioxide, nitrogen oxides, and ammonia, *Atmos. Chem. Phys.*, *13*(5), 2635–2652, doi:10.5194/acp-13-2635-2013.

Wang, Y., Q. Zhang, J. Jiang, W. Zhou, B. Wang, K. He, F. Duan, Q. Zhang, S. Philip, and Y. Xie (2014), Enhanced sulfate formation during China's severe winter haze episode in January 2013 missing from current models, *J. Geophys. Res. Atmos.*, *119*, 10,425–410,440, doi:10.1002/2013JD021426.

Wang, Y. Q., X. Y. Zhang, J. Y. Sun, X. C. Zhang, H. Z. Che, and Y. Li (2015), Spatial and temporal variations of the concentrations of PM10, PM2.5 and PM1 in China, *Atmos. Chem. Phys.*, *15*(23), 13,585–13,598, doi:10.5194/acp-15-13585-2015.

Wesely, M. L. (1989), Parameterization of surface resistances to gaseous dry deposition in regional-scale numerical models, *Atmos. Environ.*, *23*(6), 1293–1304, doi:10.1016/0004-6981(89)90153-4.

West, J. J., S. J. Smith, R. A. Silva, V. Naik, Y. Zhang, Z. Adelman, M. M. Fry, S. Anenberg, L. W. Horowitz, and J.-F. Lamarque (2013), Co-benefits of mitigating global greenhouse gas emissions for future air quality and human health, *Nature Clim. Change*, *3*(10), 885–889, doi:10.1038/nclimate2009.

Westervelt, D. M., L. W. Horowitz, V. Naik, and D. L. Mauzerall (2015), Radiative forcing and climate response to projected 21st century aerosol decreases, *Atmos. Chem. Phys.*, *15*(22), 12,681–12,703, doi:10.5194/acp-15-12681-2015.

World Health Organization (2005), WHO air quality guidelines global update, report on a working group meeting Bonn, Germany, 18–20 October, 2005, *Rep. E87950*, 25 pp., Geneva, Switzerland.

Xing, J., R. Mathur, J. Pleim, C. Hogrefe, C. M. Gan, D. C. Wong, C. Wei, R. Gilliam, and G. Pouliot (2015), Observations and modeling of air quality trends over 1990–2010 across the Northern Hemisphere: China, the United States and Europe, *Atmos. Chem. Phys.*, *15*(5), 2723–2747, doi:10.5194/acp-15-2723-2015.

Xing, J., S. X. Wang, S. Chatani, C. Y. Zhang, W. Wei, J. M. Hao, Z. Klimont, J. Cofala, and M. Amann (2011), Projections of air pollutant emissions and its impacts on regional air quality in China in 2020, *Atmos. Chem. Phys.*, *11*(7), 3119–3136, doi:10.5194/acp-11-3119-2011.

Xu, L., et al. (2015), Effects of anthoropogenic emissions on aerosol formation from isoprene and monoterpenes in the southeastern United States, *Proc. Natl. Acad. Sci. U.S.A.*, *112*(1), 37–42, doi:10.1073/pnas.1417609112.

Yan, Y., J. Lin, J. Chen, and L. Hu (2016), Improved simulation of tropospheric ozone by a global-multi-regional two-way coupling model system, *Atmos. Chem. Phys.*, *16*(4), 2381–2400, doi:10.5194/acp-16-2381-2016.

Yang, Y., H. Liao, and S. J. Lou (2015), Decadal trend and interannual variation of outflow of aerosols from East Asia: Roles of variations in meteorological parameters and emissions, *Atmos. Environ.*, *100*, 141–153, doi:10.1016/j.atmosenv.2014.11.004.

Yienger, J. J., and H. Levy (1995), Empirical model of global soil-biogenic NOx emissions, *J. Geophys. Res.*, *100*(D6), 11,447–11,464, doi:10.1029/95JD00370.

Zhang, L., H. Liao, and J. Li (2010), Impacts of Asian summer monsoon on seasonal and interannual variations of aerosols over eastern China, *J. Geophys. Res.*, *115*, D00K05, doi:10.1029/2009JD012299.

Zhang, L., D. J. Jacob, N. V. Downey, D. A. Wood, D. Blewitt, C. C. Carouge, A. van Donkelaar, D. B. A. Jones, L. T. Murray, and Y. Wang (2011), Improved estimate of the policy-relevant background ozone in the United States using the GEOS-Chem global model with 1/2° × 2/3° horizontal resolution over North America, *Atmos. Environ.*, *45*(37), 6769–6776, doi:10.1016/j.atmosenv.2011.07.054.

Zhang, L., L. C. Liu, Y. H. Zhao, S. L. Gong, X. Y. Zhang, K. H. Daven, L. C. Shannon, T. M. Fu, Q. Zhang, and Y. X. Wang (2015a), Source attribution of particulate matter pollution over North China with the adjoint method, *Environ. Res. Lett.*, *10*(8), 084,011, doi:10.1088/1748-9326/10/8/084011.

Zhang, L., T. Wang, M. Lv, and Q. Zhang (2015b), On the severe haze in Beijing during January 2013: Unraveling the effects of meteorological anomalies with WRF-Chem, *Atmos. Environ.*, *104*(0), 11–21, doi:10.1016/j.atmosenv.2015.01.001.

Zhang, Q., et al. (2009), Asian emissions in 2006 for the NASA INTEX-B mission, *Atmos. Chem. Phys.*, *9*(14), 5131–5153, doi:10.5194/acp-9-5131-2009.

Zhang, X. Y., J. J. Cao, L. M. Li, R. Arimoto, Y. Cheng, B. Huebert, and D. Wang (2002), Characterization of atmospheric aerosol over XiAn in the south margin of the Loess Plateau, China, *Atmos. Environ.*, *36*(26), 4189–4199, doi:10.1016/S1352-2310(02)00347-3.

Zhang, X. Y., Y. Q. Wang, T. Niu, X. C. Zhang, S. L. Gong, Y. M. Zhang, and J. Y. Sun (2012), Atmospheric aerosol compositions in China: Spatial/temporal variability, chemical signature, regional haze distribution and comparisons with global aerosols, *Atmos. Chem. Phys.*, *12*(2), 779–799, doi:10.5194/acp-12-779-2012.

Zhu, J., and H. Liao (2016), Future ozone air quality and radiative forcing over China owing to future changes in emissions under the Representative Concentration Pathways (RCPs), *J. Geophys. Res. Atmos.*, *121*, 1978–2001, doi:10.1002/2015JD023929.

Zhu, J., H. Liao, and J. Li (2012), Increases in aerosol concentrations over eastern China due to the decadal-scale weakening of the East Asian summer monsoon, *Geophys. Res. Lett.*, *39*, L09809, doi:10.1029/2012GL051428.

Zhuang, X., Y. Wang, H. He, J. Liu, X. Wang, T. Zhu, M. Ge, J. Zhou, G. Tang, and J. Ma (2014), Haze insights and mitigation in China: An overview, *J. Environ. Sci.*, *26*(1), 2–12, doi:10.1016/S1001-0742(13)60376-9.